

Supporting information

Organic Solar Cells with 20.12% Efficiency Enabled by Monosubstituted Carbazole-based Self-Assembled Monolayers

Qiaonan Chen,^{1, †} Jingnan Wu,^{1, †} Maureen Gumbo,¹ Leandro R. Franco,^{1, 2} Kangbo Sun,³ Lunjie Zeng,⁴ Xianjie Liu,⁵ Yufei Wang,³ Donghong Yu,^{6,7,11} Lars Öhrström,¹ Mailde S. Ozório,⁸ Alexandre Holmes,¹ C. Moyses Araujo,^{2, 9} Eva Olsson,³ Mats Fahlman,⁴ Renqiang Yang¹⁰ * and Ergang Wang^{1, 11} *

¹Department of Chemistry and Chemical Engineering, Chalmers University of Technology, Göteborg, SE-412 96, Sweden

²Department of Engineering and Physics, Karlstad University, Karlstad 65188, Sweden

³College of New Materials and New Energies, Shenzhen Technology University, Shenzhen 518118, China

⁴Department of Physics, Chalmers University of Technology, Göteborg, SE-412 96, Sweden

⁵Laboratory of Organic Electronics (LOE), Department of Science and Technology, Linköping University, 60174 Norrköping, Sweden

⁶Department of Chemistry and Bioscience, Aalborg University, Aalborg, DK-9220, Denmark

⁷Sino-Danish Center for Education and Research, Aarhus, DK-8000, Denmark

⁸Department of Chemistry, University of Copenhagen, DK-1350, Denmark

⁹Materials Theory Division, Department of Physics and Astronomy, Uppsala University, Uppsala 75120, Sweden

¹⁰Key Laboratory of Optoelectronic Chemical Materials and Devices (Ministry of Education) School of Optoelectronic Materials and Technology, Jiangnan University, Wuhan 430056, China

¹¹School of Materials Science and Engineering, Zhengzhou University, Zhengzhou 450001, China

†These authors contributed equally.

*Corresponding author. E-mail: Renqiang Yang, yangrq@jhun.edu.cn, Ergang Wang, ergang@chalmers.se

Table of Contents

1. Materials and Methods
2. Synthesis and Characterization
3. Supporting Figures S1 to S19 & Tables S1 to S11
4. Nuclear Magnetic Resonance (NMR) Spectra, Figures S20 to S49
5. Supporting References

1. Materials and Methods

Materials:

1,2-Dibromoethane, tetrabutylammonium bromide, triethyl phosphite and bromotrimethylsilane were purchased from Sigma-Aldrich. 3-Fluorocarbazole, 3-chloro-9H-carbazole, 3-bromocarbazole and 3-iodocarbazole were purchased from VWR. PM6 was purchased from Solarmer Materials Inc and eFlexPV Limited, respectively. L8-BO and PDINN were acquired from eFlexPV Limited. ITO glass substrates for UPS and XPS measurement were purchased Ossila Ltd. ITO glass substrates for photovoltaic measurement were purchased South China Science & Technology Company Limited. All the other reagents and chemicals were purchased from Sigma-Aldrich or Fisher and used as received.

Methods:

^1H and ^{13}C NMR spectra were recorded on 600MHz Oxford magnet equipped with Bruker NEO console and QCIIP $^1\text{H}/^{19}\text{F}/^{31}\text{P}/^{13}\text{C}/^{15}\text{N}$ cold probe, with residual solvent signals as internal reference (^1H NMR: DMSO- d_6 , 2.50 ppm; $^{13}\text{C}\{^1\text{H}\}$ NMR: DMSO- d_6 , 39.52 ppm). The following abbreviations are used to describe peak patterns: br = broad signal, s = singlet, d = doublet, t = triplet, dd = doublet of doublets, m = multiplet. The ultraviolet-visible (UV-vis) absorption spectra were recorded on a PerkinElmer lambda 1050 UV/Vis/NIR spectrometer. Thermogravimetric analysis (TGA) was conducted by a Mettler Toledo TGA/DSC 3+ STAR System instrument under nitrogen atmosphere at a heating rate of $10\text{ }^\circ\text{C min}^{-1}$. Differential scanning calorimetry (DSC) measurement was performed by using DSC 250 (TA Instruments). DSC and TGA measurements were carried out on the powdered product of the SAMs. Ultraviolet photoelectron spectroscopy (UPS) measurements were performed by a Thermo Fisher Scientific K-ALPHA+ system with He I (21.2 eV) as the excitation source. X-ray photoelectron spectroscopy (XPS) (Thermo Scientific K-Alpha) for the analysis of materials' elemental composition is utilized. The morphology of ITO surface was investigated by using a Zeiss Leo Ultra 55 scanning electron microscope (SEM) at an beam energy of 20 kV. A JEOL monochromated ARM200F transmission electron microscopy (TEM) microscope operated at 200 kV was used for scanning transmission electron microscopy (STEM) analysis. The

microscope is equipped with a double-Wien monochromator, probe and image C_s aberration correctors, and high-angle annular darkfield (HAADF) STEM detectors. Atomic-resolution HAADF STEM imaging was used to directly visualize the SAMs-modified ITO structure. For STEM analysis, a Leica EM ACE 600 sputter coater was used to deposit a Au layer with a thickness of ~ 10 nm on the surfaces of SAMs-modified ITO. Cross-sectional STEM specimens were then prepared by using a FEI Versa 3D focus ion beam – scanning electron microscope (FIB-SEM). Atomic force microscopy (AFM) was performed through standard tapping-mode in ambient air on a scanned probe imaging and development (SPID) Park NX-10 imaging system. The AFM images were confirmed from different samples and scan areas. The root-mean-square roughness (RMS) values of the height images were obtained from the entire scan area ($2 \times 2 \mu\text{m}^2$). All AFM images were flattened and exported from the software (XEI). Contact angles of distinct solutions (deionized water and diiodomethane) on hole transport layer films were measured by using Dataphysics-OCA20 Micro surface contact angle analyzer.

OSCs Fabrication:

The normal type OSCs (indium-tin-oxide (ITO)/SAMs/active layer/interlayer/Ag) were fabricated by following processes: N,N'-Bis[3-(dimethylamino)propyl]perylene-3,4,9,10-tetracarboxylic Diimide (PDINN) was used as interfacial layer. ITO-coated glass substrates were treated with ultrasonication by DI-water, acetone, and isopropyl alcohol. The cleaned substrates were dried for more than 1 hr at 80°C . Such pre-cleaned ITO substrates were treated in UV-ozone for 25 min before spin-casting SAMs. The ethanol solution of SAMs (0.3 mg/mL) was spin-casted at 3000 rpm for 30 s and then thermally annealed at 85°C for 5 min in ambient condition. Subsequently, the SAMs solution was spin-cast twice at 6000 rpm for 30 seconds each. Then, they were transferred to a N_2 -filled glovebox. Next, the PM6:L8-BO blend solutions with optimal P_D concentration (7 mg mL^{-1}) and $P_D:P_A$ ratio (1:1.2) were prepared in chloroform. The solutions were stirred for at least 0.5 hr at 45°C , and the 0.75% vol 1-chloronaphthalene was added before spin-coating. Then, solutions were spin-casted onto the SAM-coated ITO substrates at 3000 rpm for 30 s, and the films were thermally annealed at 85°C for 5 min. Then, PDINN with a methanol solution at a concentration of 1 mg mL^{-1} was spin-coated onto the active layer films with 3000 rpm for 30 s. Finally, Ag electrode (100 nm) was

deposited by thermal evaporation in an evaporation chamber, under a high vacuum ($\sim 10^{-5}$ Torr) condition. The photoactive area of the OSC devices is 0.042 cm^2 , measured from the optical microscopy. The mask area for measurement is 0.0225 cm^2 .

OSCs Measurements:

The current density-voltage (J - V) curves of all encapsulated devices were measured using a Keithley 2400 Source Meter under AM 1.5G (100 mW cm^{-2}) using an Enlitech solar simulator. The light intensity was calibrated using a standard Si diode with KG5 filter to bring spectral mismatch to unity. Optical microscope (Olympus BX51) was used to define the device area (7.2 mm^2). The external quantum efficiency (EQE) was measured by using a solar cell spectral response measurement system QE-R3011 of Enli Technology CO., Ltd. A digital oscilloscope was used to acquire the TPV signal at the open-circuit condition. The impedance spectrum, capacitance-frequency, and Photo-CELIV measurements were performed using commercially available Paios system (FLUXiM AG). The contact angle images of films were obtained from Optical contact angle measuring and contour analysis systems (OCA 15EC).

SCLC Measurement:

The hole-only devices for the SCLC measurement have device architectures of ITO/SAMs/active layer (100 nm)/MoO₃ (10 nm)/Ag. The semiconducting films were spin-casted in the N₂-filled glovebox, and the blend films were prepared in the same condition as that for OSCs fabrication. Mott-Gurney equation was used to fit the J - V characteristics:

$$J_{SCLC} = \frac{9}{8} \epsilon_0 \epsilon_r \mu (V^2/L^3).$$

(ϵ_0 = the free-space permittivity, ϵ_r = the dielectric constant of the semiconductor, μ = the mobility, V = the applied voltage, and L = the thickness of the active layer.)

Surface energy calculation of film

The solid surface energy using Owen method was based on the following model:

$$\gamma_s = \gamma_s^D + \gamma_s^P \quad (1)$$

$$\gamma_l = \gamma_l^D + \gamma_l^P \quad (2)$$

where γ_s stands for the surface of the solid, which consists of the polarity force γ_s^P and dispersion force γ_s^D , and γ_l refers to the surface energy of the liquid with the corresponding polarity force γ_l^P and dispersion force γ_l^D . According to the following equation, the γ_s^P and γ_s^D of measured film can be acquired.

$$\gamma_l(1 + \cos\theta) = 2(\gamma_s^D \gamma_l^D)^{1/2} + 2(\gamma_s^P \gamma_l^P)^{1/2} \quad (3)$$

In this work, the water (H₂O) and diiodomethane (DIM) are used as the testing liquids to extract the γ_s^P and γ_s^D . The related parameters of H₂O and DIM are listed in Table S7.

GIWAXS Characterization

GIWAXS characterization was conducted by 2D-GIWAXS experiments using a GANESHA 300XL+ system from JJ X-ray. The instrument is equipped with a Pilatus 300K detector with a pixel size of 172 × 172 μm. The X-ray source is a Genix 3D Microfocus sealed tube X-Ray Cu-source with an integrated monochromator (30 W). The wavelength used was $\lambda = 1.5418 \text{ \AA}$. The detector moved in a vacuum chamber with a sample-to-detector distance varied between 0.115 m and 1.47 m, depending on the configuration, as calibrated by silver behenate ($d_{001} = 58.380 \text{ \AA}$). The minimized background scattering plus high-performance detector allowed for a detectable q -range varying from 3×10^{-4} to 3 \AA^{-1} (0.2 to 210 nm). The sample was placed vertically on the goniometer and tilted to a glancing angle of 0.2° with respect to the incoming beam. A small beam was then used to obtain better resolution. The accumulation time was 30 min for each measurement. In-plane and out-of-plane line-cuts were obtained using the SAXSGUI program.

Single-Crystal X-ray Diffraction Analysis

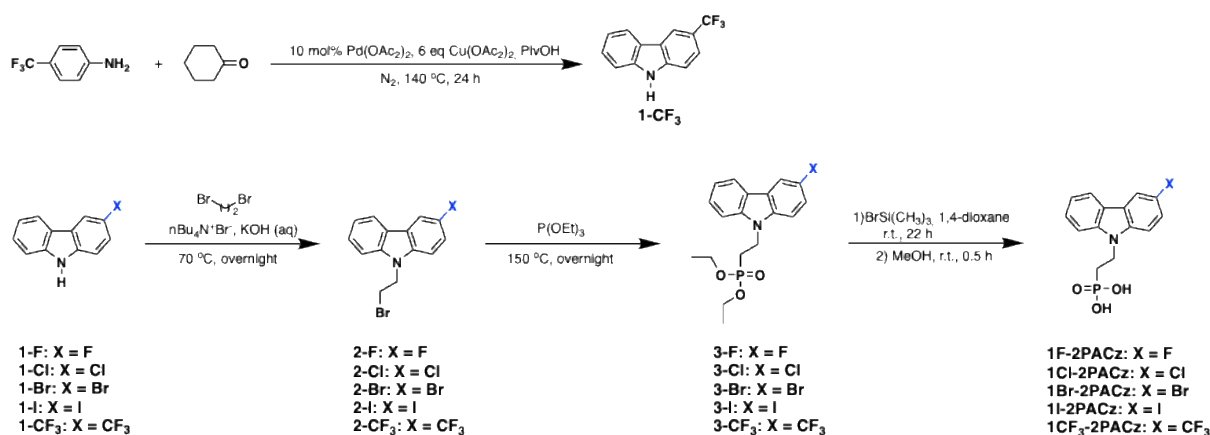
Experiments were carried out with Cu $K\alpha$ radiation. Single metallic light colourless block-shaped crystals of 1F-2PACz, 1Br-2PACz, 1I-2PACz, and 1I-carbazole were obtained by recrystallisation from ethanol. Suitable crystals were selected and placed on a mounted cryo loop on an XtaLAB Synergy R, HyPix diffractometer. The crystal was kept at a steady at constant temperature during data collection. The structure was solved with the ShelXT 2014/5 (Sheldrick, 2014) structure solution program using the Intrinsic Phasing solution method and

by using Olex2 (Dolomanov et al., 2009) as the graphical interface.¹ The model was refined with version 2016/6 of ShelXL 2016/6 (Sheldrick, 2015) using Least Squares minimisation.

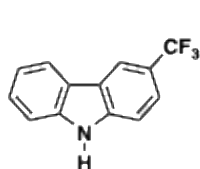
Theoretical Modeling

The electronic structure of 1X-2PACz (X = F, Cl, Br, I, CF₃) molecules was systematically investigated using Density Functional Theory (DFT) and Time-Dependent DFT (TD-DFT) methods. Geometry optimizations and all the electronic properties calculations were performed at the B3LYP²/6-311G(d,p)³ theory level. For simplicity, the P(OH)₂O group was substituted by a hydrogen atom. The energy levels of the systems were determined by calculating the energy of the frontier molecular orbitals and the energy of the first electronic transition (S1). The molecular calculations were carried out using the Gaussian 16 program (Rev C.01).⁴ Density functional theory calculations were performed to obtain the work function of ITO with and without adsorbed 1X-2PACz (X = F, Cl, Br, I, CF₃) molecules. The ITO was modeled using a slab with In₆₀Sn₄O₉₆ stoichiometry, featuring approximately 27 Å of vacuum along the z-axis. The molecules were adsorbed on only one side of the slab. To solve the Kohn-Sham equations, we utilized the Perdew-Burke-Ernzerhof (PBE) generalized gradient approximation⁵ in conjunction with the all-electron projector augmented-wave (PAW) method^{6, 7}. The equilibrium volume of the In₆₀Sn₄O₉₆ slabs with and without adsorbed molecules was found by optimizing the stress tensor and atomic forces within a plane-wave cutoff energy of 600 eV along the integration over the Brillouin zone using a k-mesh of 5×5×1. The equilibrium crystal structures were reached once the atomic forces on every atom were smaller than 0.010 eV/Å and using self-consistent criteria of 10⁻⁵ eV for the total energy. To obtain the work function, the precision of the calculations was increased by using a k-mesh of 7×7×1 and by including the D3 van der Waals correction⁸. The calculations were carried out using the Vienna *ab initio* simulation package (VASP)^{9, 10} version 5.4.1.

2. Synthesis and Characterization



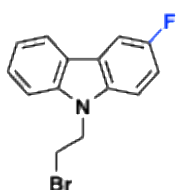
Scheme S1. Synthesis route of 1F-, 1Cl-, 1Br-, 1I-, and 1CF₃-2PACz.¹¹



3-(trifluoromethyl)-9H-carbazole (1-CF₃)¹²

To a 50 mL Schlenk tube equipped with a magnetic stirrer, aniline (705 mg, 4.37 mmol), cyclohexanone (329 μ L, 9.37 mmol), Pd(OAc)₂ (10 mol%), Cu(OAc)₂ (6 eq), and PivOH (12.5 mL) were added. The reaction vessel was cooled with liquid nitrogen, degassed under vacuum and refilled with N₂. This procedure was repeated three times. The reaction mixture was stirred at 140 °C for 24 h. After cooling to room temperature, the reaction mixture was diluted with saturated aqueous solution of K₂CO₃, and extracted with EtOAc, the combined organic layer was dried over Na₂SO₄, filtered, and evaporated under vacuum. The residue was purified by column chromatography on silica gel (hexane : ethyl acetate = 2:1) to afford the desired product **1-CF₃** as white shining solid in 330 mg, 45% yield.

¹H NMR (600 MHz, DMSO-*d*₆, TMS) δ (ppm): 11.72 (s, 1H), 8.57 (s, 1H), 8.29 (d, *J* = 7.8 Hz, 1H), 7.72-7.64 (m, 2H), 7.57 (d, *J* = 8.2 Hz, 1H), 7.47 (t, *J* = 7.6 Hz, 1H), 7.23 (t, *J* = 7.4 Hz, 1H). ¹³C NMR (150 MHz, DMSO-*d*₆, TMS), δ (ppm): 141.5, 140.4, 126.7, 126.5, 124.7, 122.1, 122.0, 120.9, 119.5, 119.3, 119.1, 118.0, 111.5.

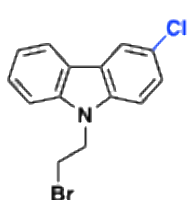


9-(2-bromoethyl)-3-fluoro-9H-carbazole (2-F)

3-Fluoro-9H-carbazole (**1-F**, 1 eq, 1.24 g, 6.7 mmol) was dissolved in 1,2-dibromoethane (17 eq, 20 g, 115 mmol), followed by the sequential addition of tetrabutylammonium bromide (0.14 eq, 301 mg, 0.94 mmol) and 50% aqueous KOH solution (4.6 eq, 1.73 g, 30.8 mmol). Reaction was stirred at 70 °C overnight. TLC analysis reveals that

starting material **1-F** remains present in the reaction mixture. Extra tetrabutylammonium bromide (520 mg) and 50% KOH aqueous solution (2.1 g) was added. The reaction was run another 24 hours. After completion of the reaction, extraction was done with chloroform. The organic layer was washed with brine for three times, dried over anhydrous Na_2SO_4 , and then the solvent was distilled off under reduced pressure. The crude product was purified by column chromatography (silica gel: 70 to 230 mesh; eluent: petroleum ether first to remove residual 1,2-dibromoethane, then petroleum ether: chloroform 6:1 v:v) to give **2-F** as a white solid in 1.25 g, 64% yield.

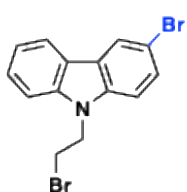
^1H NMR (600 MHz, $\text{DMSO}-d_6$, TMS), δ (ppm): 8.17 (d, $J = 7.4$ Hz, 1H), 8.01 (dd, $J = 9.2, 2.6$ Hz, 1H), 7.70 – 7.64 (m, 2H), 7.51 – 7.46 (m, 1H), 7.31 (td, $J = 9.2, 2.7$ Hz, 1H), 7.21 (t, $J = 7.4$ Hz, 1H), 4.85 (t, $J = 6.3$ Hz, 2H), 3.90 (t, $J = 6.3$ Hz, 2H). ^{13}C NMR (150 MHz, $\text{DMSO}-d_6$, TMS), δ (ppm): 157.5, 156.0, 140.8, 136.4, 126.4, 122.8, 122.7, 121.8, 120.8, 119.1, 113.3, 113.2, 110.7, 110.6, 109.9, 106.0, 105.9, 44.1, 31.3.



9-(2-bromoethyl)-3-chloro-9H-carbazole (2-Cl)

The same procedure as the synthesis of **2-F** was applied on 3-chloro-9H-carbazole (**1-Cl**) for yielding 9-(2-bromoethyl)-3-chloro-9H-carbazole (**2-Cl**) in form of white solids (1.7 g, 44% yield).

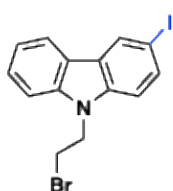
^1H NMR (600 MHz, $\text{DMSO}-d_6$, TMS), δ (ppm): 8.27 (d, $J = 2.2$ Hz, 1H), 8.21 (dd, $J = 7.8, 0.8$ Hz, 1H), 7.70 (d, $J = 8.7$ Hz, 1H), 7.67 (d, $J = 8.3$ Hz, 1H), 7.52 – 7.48 (m, 1H), 7.46 (dd, $J = 8.7, 2.1$ Hz, 1H), 7.24 (ddd, $J = 7.9, 7.1, 0.9$ Hz, 1H), 4.85 (t, $J = 6.3$ Hz, 2H), 3.90 (t, $J = 6.3$ Hz, 2H). ^{13}C NMR (150 MHz, $\text{DMSO}-d_6$, TMS), δ (ppm): 140.4, 138.4, 126.5, 125.4, 123.5, 121.4, 120.8, 119.9, 119.5, 111.3, 109.9, 44.0, 31.3.



3-bromo-9-(2-bromoethyl)-9H-carbazole (2-Br)

The same procedure as the synthesis of **2-F** was applied on 3-bromo-9H-carbazole (**1-Br**) for yielding 9-(2-bromoethyl)-3-bromo-9H-carbazole (**2-Br**) in form of white solids (1.15 g, 27% yield).

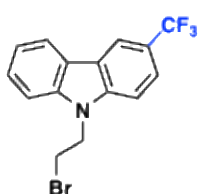
^1H NMR (600 MHz, $\text{DMSO-}d_6$, TMS), δ (ppm): 8.40 (s, 1H), 8.21 (d, $J = 7.8$ Hz, 1H), 7.72 – 7.64 (m, 2H), 7.57 (d, $J = 8.6$ Hz, 1H), 7.49 (t, $J = 7.7$ Hz, 1H), 7.24 (t, $J = 7.5$ Hz, 1H), 4.85 (t, $J = 6.3$ Hz, 2H), 3.90 (t, $J = 6.3$ Hz, 2H). ^{13}C NMR (150 MHz, $\text{DMSO-}d_6$, TMS), δ (ppm): 140.2, 138.7, 128.0, 126.6, 124.2, 122.8, 121.3, 120.8, 119.6, 111.7, 111.3, 109.9, 44.0, 31.3.



9-(2-bromoethyl)-3-iodo-9H-carbazole (2-I)

The same procedure as the synthesis of **2-F** was applied on 3-iodo-9H-carbazole (**1-I**) for yielding 9-(2-bromoethyl)-3-iodo-9H-carbazole (**2-I**) in form of white solids (1.22 g, 35% yield).

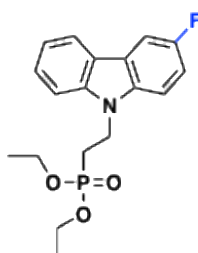
^1H NMR (600 MHz, $\text{DMSO-}d_6$, TMS), δ (ppm): 8.55 (s, 1H), 8.20 (d, $J = 7.8$ Hz, 1H), 7.71 (d, $J = 8.5$ Hz, 1H), 7.67 (d, $J = 8.3$ Hz, 1H), 7.55 (d, $J = 8.6$ Hz, 1H), 7.51 – 7.46 (m, 1H), 7.23 (t, $J = 7.4$ Hz, 1H), 4.84 (t, $J = 6.3$ Hz, 2H), 3.90 (t, $J = 6.2$ Hz, 2H). ^{13}C NMR (150 MHz, $\text{DMSO-}d_6$, TMS), δ (ppm): 139.9, 139.2, 133.5, 128.7, 126.5, 124.9, 121.0, 120.7, 119.6, 112.2, 109.8, 82.17, 43.9, 31.3.



9-(2-bromoethyl)-3-(trifluoromethyl)-9H-carbazole (2-CF₃)

The same synthesizing procedure as the synthesis of **2-F** was applied on 3-(trifluoromethyl)-9H-carbazole (**1-CF₃**) for yielding 9-(2-bromoethyl)-3-(trifluoromethyl)-9H-carbazole (**2-CF₃**) in form of white solids (0.57 g, 47% yield).

^1H NMR (600 MHz, $\text{DMSO-}d_6$, TMS), δ (ppm): 8.62 (s, 1H), 8.34 (d, $J = 7.8$ Hz, 1H), 7.88 (d, $J = 8.6$ Hz, 1H), 7.79 – 7.72 (m, 2H), 7.55 (ddd, $J = 8.3, 7.1, 1.2$ Hz, 1H), 7.33 – 7.28 (m, 1H), 4.93 (t, $J = 6.2$ Hz, 2H), 3.95 (t, $J = 6.2$ Hz, 2H). ^{13}C NMR (150 MHz, $\text{DMSO-}d_6$, TMS), δ (ppm): 141.7, 140.6, 126.8, 122.2, 122.0, 121.9, 121.0, 120.1, 119.9, 119.6, 118.0, 110.4, 110.2, 44.1, 31.3.

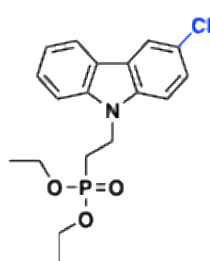


diethyl (2-(3-fluoro-9H-carbazol-9-yl)ethyl)phosphonate (3-F)

9-(2-bromoethyl)-3-fluoro-9H-carbazole (**2-F**, 1 eq, 1.25 g, 4.3 mmol) was dissolved in triethyl phosphite (20 eq, 14.20 g, 85.5 mmol). The reaction mixture was stirred at 150 °C overnight. After completion of the reaction, the

solution was evaporated under vacuum. The crude product was purified by column chromatography (silica gel: 70 to 230 mesh petroleum ether: chloroform 6:1 v:v, then acetone: petroleum ether 1:3 v:v) to give **3-F** as white solid in 0.78 g, 52% yield.

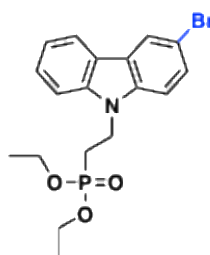
^1H NMR (600 MHz, $\text{DMSO-}d_6$, TMS), δ (ppm): 8.16 (d, $J = 7.8$ Hz, 1H), 8.00 (dd, $J = 9.2, 2.6$ Hz, 1H), 7.62 – 7.54 (m, 2H), 7.49 (t, $J = 7.7$ Hz, 1H), 7.32 (td, $J = 9.2, 2.6$ Hz, 1H), 7.21 (t, $J = 7.4$ Hz, 1H), 4.59 (dt, $J = 14.1, 7.2$ Hz, 2H), 3.88 (p, $J = 7.1$ Hz, 4H), 2.28 (dt, $J = 18.1, 7.2$ Hz, 2H), 1.08 (t, $J = 7.1$ Hz, 6H). ^{13}C NMR (150 MHz, $\text{DMSO-}d_6$, TMS), δ (ppm): 157.5, 155.9, 140.4, 136.0, 126.4, 122.8, 121.9, 120.8, 118.9, 113.3, 113.1, 110.3, 110.3, 109.6, 106.1, 105.9, 61.1, 36.8, 24.7, 23.8, 16.0.



diethyl (2-(3-chloro-9H-carbazol-9-yl)ethyl)phosphonate (3-Cl)

The same synthesizing procedure as **3-F**. White solids as **3-Cl** in 0.38 g with 21% yield were obtained.

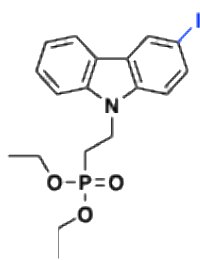
^1H NMR (600 MHz, $\text{DMSO-}d_6$, TMS), δ (ppm): 8.26 (dd, $J = 2.1, 0.5$ Hz, 1H), 8.20 (dt, $J = 7.9, 0.9$ Hz, 1H), 7.59 (t, $J = 8.9$ Hz, 2H), 7.50 (ddd, $J = 8.3, 7.1, 1.3$ Hz, 1H), 7.47 (dd, $J = 8.7, 2.1$ Hz, 1H), 7.23 (ddd, $J = 7.9, 7.1, 0.9$ Hz, 1H), 4.59 (dt, $J = 14.2, 7.2$ Hz, 2H), 3.87 (dq, $J = 8.0, 7.1, 0.8$ Hz, 4H), 2.34 – 2.24 (m, 2H), 1.07 (t, $J = 7.1$ Hz, 6H). ^{13}C NMR (150 MHz, $\text{DMSO-}d_6$, TMS), δ (ppm): 140.0, 138.0, 126.5, 125.4, 123.6, 123.4, 121.4, 120.8, 119.9, 119.4, 110.9, 109.6, 61.2, 36.8, 24.6, 23.7, 16.0.



diethyl (2-(3-bromo-9H-carbazol-9-yl)ethyl)phosphonate (3-Br)

The same synthesizing procedure as **3-F**. White solid as **3-Br** in 0.91 g with 73% yield were obtained.

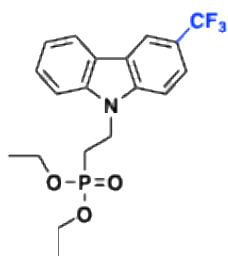
^1H NMR (600 MHz, $\text{DMSO-}d_6$, TMS), δ (ppm): 8.40 (d, $J = 2.0$ Hz, 1H), 8.21 (d, $J = 7.8$ Hz, 1H), 7.61 – 7.55 (m, 3H), 7.52 – 7.48 (m, 1H), 7.23 (t, $J = 7.0$ Hz, 1H), 4.58 (dt, $J = 14.2, 7.1$ Hz, 2H), 3.87 (p, $J = 7.4$ Hz, 4H), 2.28 (dt, $J = 18.0, 7.2$ Hz, 2H), 1.07 (t, $J = 7.0$ Hz, 6H). ^{13}C NMR (150 MHz, $\text{DMSO-}d_6$, TMS), δ (ppm): 139.9, 138.3, 128.0, 126.5, 124.2, 122.8, 121.3, 120.8, 119.4, 111.4, 111.1, 109.6, 61.15, 61.1, 36.8, 24.6, 23.7, 16.0, 16.0.



diethyl (2-(3-iodo-9H-carbazol-9-yl)ethyl)phosphonate (3-I)

The same synthesizing procedure as **3-F**. White solids as **3-I** in 0.79 g with 61% yield were obtained.

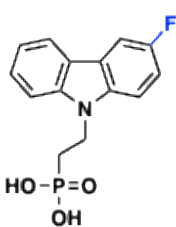
^1H NMR (600 MHz, DMSO- d_6 , TMS), δ (ppm): 8.55 (s, 1H), 8.19 (d, $J = 7.7$ Hz, 1H), 7.72 (d, $J = 8.7$ Hz, 1H), 7.58 (d, $J = 8.2$ Hz, 1H), 7.49 (t, $J = 7.5$ Hz, 1H), 7.44 (d, $J = 8.7$ Hz, 1H), 7.23 (t, $J = 7.4$ Hz, 1H), 4.57 (dt, $J = 14.2, 7.2$ Hz, 2H), 3.87 (p, $J = 8.0$ Hz, 4H), 2.27 (dt, $J = 18.2, 7.2$ Hz, 2H), 1.07 (t, $J = 7.1$ Hz, 6H). ^{13}C NMR (150 MHz, DMSO- d_6 , TMS), δ (ppm): 139.5, 138.7, 133.5, 128.7, 126.5, 125.0, 121.1, 120.8, 119.4, 111.9, 109.5, 82.0, 61.1, 36.7, 24.6, 23.7, 16.0.



diethyl (2-(3-(trifluoromethyl)-9H-carbazol-9-yl)ethyl)phosphonate (3-CF₃)

The same synthesizing procedure as **3-F**. White solids as **3-CF₃** in 0.37 g with 17% yield were obtained.

^1H NMR (600 MHz, DMSO- d_6 , TMS), δ (ppm): 8.60 (d, $J = 1.0$ Hz, 1H), 8.33 (d, $J = 7.7$ Hz, 1H), 7.77 (d, $J = 1.2$ Hz, 2H), 7.66 (d, $J = 8.3$ Hz, 1H), 7.55 (ddd, $J = 8.3, 7.1, 1.2$ Hz, 1H), 7.30 (ddd, $J = 7.9, 7.1, 0.9$ Hz, 1H), 4.66 (dt, $J = 14.4, 7.1$ Hz, 2H), 3.86 (p, $J = 7.2$ Hz, 4H), 2.33 (dt, $J = 18.0, 7.1$ Hz, 2H), 1.05 (t, $J = 7.0$ Hz, 6H). ^{13}C NMR (150 MHz, DMSO- d_6 , TMS), δ (ppm): 141.3, 140.2, 126.8, 122.2, 122.1, 122.0, 121.0, 119.9, 119.7, 119.5, 117.97, 110.1, 109.9, 61.2, 61.1, 36.9, 24.6, 23.7, 16.0, 15.9.

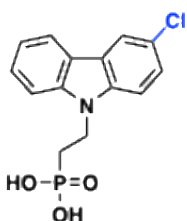


(2-(3-fluoro-9H-carbazol-9-yl)ethyl)phosphonic acid (1F-2PACz)

In a 50 mL dry round-bottom flask, diethyl (2-(3-fluoro-9H-carbazol-9-yl)ethyl)phosphonate (**3-F**, 1 eq, 690 mg, 2.0 mmol) was dissolved in anhydrous 1,4-dioxane (16.5 mL) under nitrogen atmosphere and bromotrimethylsilane (10 eq, 3.02 g, 2.61 mL, 20.0 mmol) was added dropwise. The reaction was stirred for 12 h at room temperature under nitrogen atmosphere. Afterwards most solvent was removed under reduced pressure, and the viscous liquid residue was dissolved in methanol (5 mL) and stirred for 0.5 hr. Next, distilled water was added dropwise (50 mL), until solution

became opaque and stirred for another 12 hr. Product was filtered off and washed with water to give **1F-2PACz** as white solids in 160 mg, 28% yield.

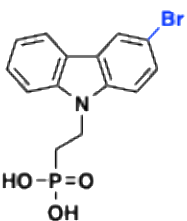
^1H NMR (600 MHz, DMSO- d_6 , TMS), δ (ppm): 8.17 (d, $J = 6.7$ Hz, 1H), 8.01 (dd, $J = 9.2, 2.6$ Hz, 1H), 7.55 (dd, $J = 8.5, 3.8$ Hz, 2H), 7.49 (ddt, $J = 8.3, 7.0, 1.3$ Hz, 1H), 7.33 (td, $J = 9.2, 2.7$ Hz, 1H), 7.24 – 7.18 (m, 1H), 4.60 – 4.50 (m, 2H), 2.08 – 1.96 (m, 2H). ^{13}C NMR (150 MHz, DMSO- d_6 , TMS), δ (ppm): 157.5, 155.9, 140.3, 136.0, 126.5, 122.8, 121.9, 120.9, 118.9, 113.5, 113.3, 110.0, 109.9, 109.3, 106.2, 106.1, 37.6, 27.7, 26.9.



(2-(3-chloro-9H-carbazol-9-yl)ethyl)phosphonic acid (1Cl-2PACz)

The same synthesizing procedure as **1F-2PACz**. White solids in 170 mg, 74% yield.

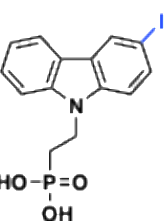
^1H NMR (600 MHz, DMSO- d_6 , TMS), δ (ppm): 8.27 (d, $J = 2.2$ Hz, 1H), 8.20 (d, $J = 7.7$ Hz, 1H), 7.56 (t, $J = 7.9$ Hz, 2H), 7.53 – 7.46 (m, 2H), 7.23 (t, $J = 7.0$ Hz, 1H), 4.54 (q, $J = 8.0$ Hz, 2H), 2.09 – 1.97 (m, 2H). ^{13}C NMR (150 MHz, DMSO- d_6 , TMS), δ (ppm): 140.0, 137.9, 126.7, 125.5, 123.6, 123.4, 121.4, 121.0, 120.0, 119.3, 110.6, 109.3, 37.6, 27.7, 26.8.



(2-(3-bromo-9H-carbazol-9-yl)ethyl)phosphonic acid (1Br-2PACz)

The same synthesizing procedure as **1F-2PACz**. White solids in 450 mg, 77% yield.

^1H NMR (600 MHz, DMSO- d_6 , TMS), δ (ppm): 8.40 (d, $J = 2.0$ Hz, 1H), 8.21 (d, $J = 7.8$ Hz, 1H), 7.59 (dd, $J = 8.6, 2.0$ Hz, 1H), 7.57 – 7.48 (m, 3H), 7.23 (t, $J = 7.4$ Hz, 1H), 4.54 (q, $J = 8.0$ Hz, 2H), 2.07 – 1.97 (m, 2H). ^{13}C NMR (150 MHz, DMSO- d_6 , TMS), δ (ppm): 139.8, 138.2, 128.1, 126.7, 124.2, 123.0, 121.3, 121.0, 119.4, 111.1, 109.3, 37.6, 27.7, 26.8.

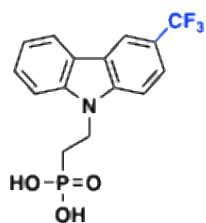


(2-(3-iodo-9H-carbazol-9-yl)ethyl)phosphonic acid (1I-2PACz)

The same synthesizing procedure as **1F-2PACz**. White solids in 340 mg, 52% yield.

^1H NMR (600 MHz, DMSO- d_6 , TMS), δ (ppm): 8.55 (s, 1H), 8.20 (d, $J = 7.7$ Hz, 1H), 7.73 (d, $J = 8.5$ Hz, 1H), 7.55 (d, $J = 8.3$ Hz, 1H), 7.53 – 7.47 (m, 1H), 7.42 (d, $J = 8.5$ Hz, 1H), 7.23 (t,

$J = 7.4$ Hz, 1H), 4.52 (q, $J = 8.0$ Hz, 2H), 2.07 – 1.97 (m, 2H). ^{13}C NMR (150 MHz, DMSO- d_6 , TMS), δ (ppm): 139.4, 138.6, 133.7, 128.9, 126.6, 125.0, 121.1, 120.9, 119.4, 111.6, 109.2, 81.9, 37.5, 27.7, 26.8.



(2-(3-(trifluoromethyl)-9H-carbazol-9-yl)ethyl)phosphonic acid (1CF₃-2PACz)

The same synthesizing procedure as **1F-2PACz**. White solids in 300 mg, 94% yield.

^1H NMR (600 MHz, DMSO- d_6 , TMS), δ (ppm): 8.61 (s, 1H), 8.34 (d, $J = 7.7$ Hz, 1H), 7.78 (d, $J = 8.8$ Hz, 1H), 7.74 (d, $J = 8.6$ Hz, 1H), 7.63 (d, $J = 8.2$ Hz, 1H), 7.56 (t, $J = 7.6$ Hz, 1H), 7.30 (t, $J = 7.4$ Hz, 1H), 4.61 (q, $J = 8.3$ Hz, 2H), 2.11 – 2.00 (m, 2H). ^{13}C NMR (150 MHz, DMSO- d_6 , TMS), δ (ppm): 141.2, 140.2, 127.0, 122.4, 122.1, 122.0, 121.2, 112.0, 119.7, 119.5, 118.1, 109.7, 109.6, 37.8, 27.7, 26.8.

3. Supporting Figures S1 to S18 & Tables S1 to S11

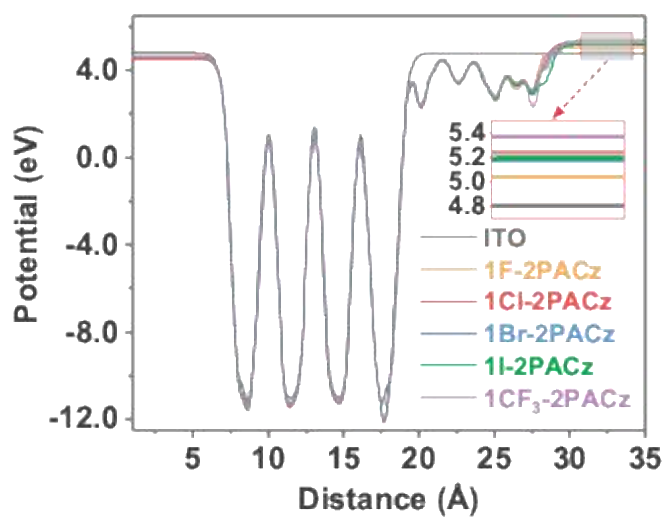


Figure S1. DFT simulated electrostatic potential energy profile for each system, with the Fermi energy level shifted to zero.

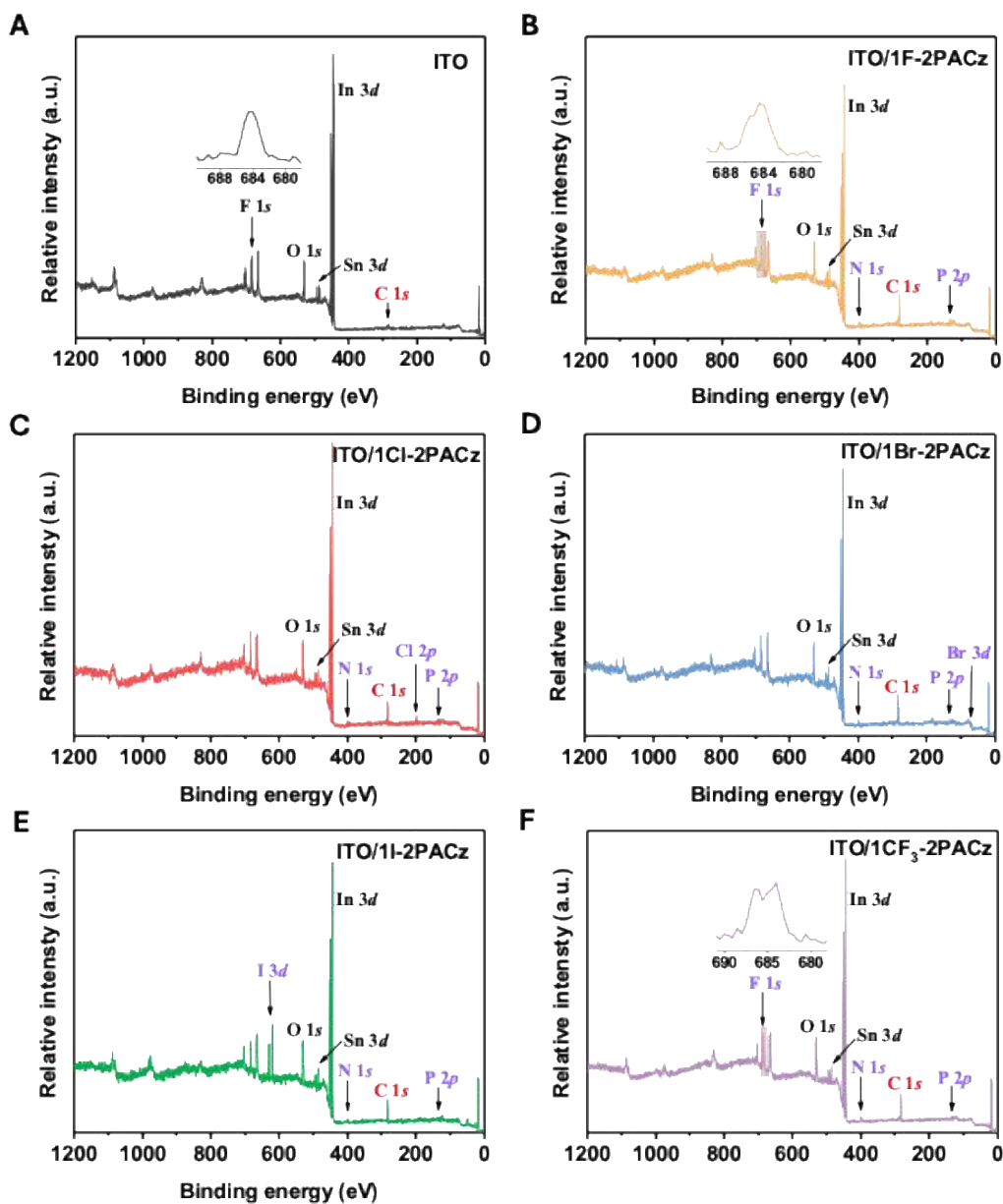


Figure S2. High-resolution X-ray photoelectron spectroscopy (HR-XPS) spectra of (A) bare ITO, (B) 1F-2PACz, (C) 1Cl-2PACz, (D) 1Br-2PACz, (E) 1I-2PACz, and (F) 1CF₃-2PACz-modified ITO.

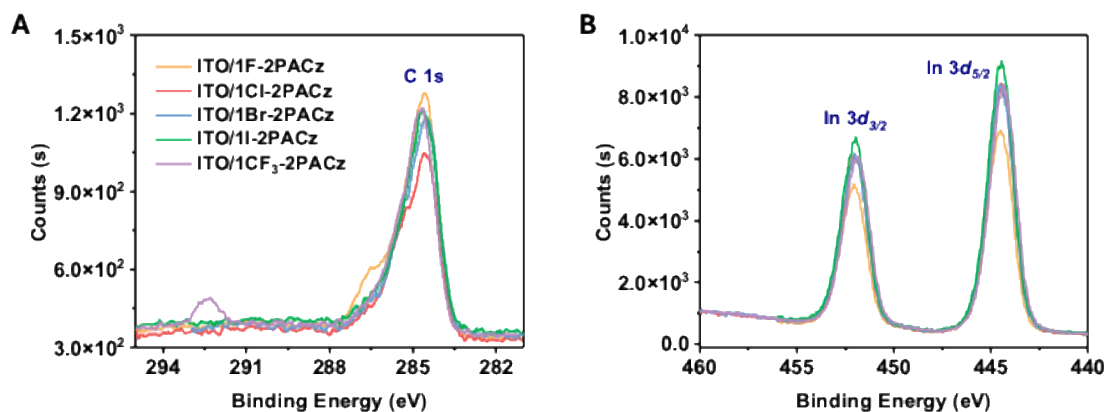


Figure S3. HR-XPS spectra of the (A) C 1s and (B) In 3d regions for SAM-modified ITO substrates.

Table S1. C 1s and In 3d_{3/2} core-level peak area as measured by HR-XPS for different SAMs-modified ITO. The C 1s peak area are divided by the number of carbon, and a relative coverage factor is calculated by normalizing to the In 3d_{3/2} core-level area.

| SAMs | XPS Peak Area | | # atoms C | Coverage Factor C 1s/14/In 3d _{3/2} |
|-------------------------|---------------|----------------------|--------------|---|
| | C 1s | In 3d _{3/2} | | |
| 1F-2PACz | 1612.9 | 7647.9 | 14 | 1.51×10^{-2} |
| 1Cl-2PACz | 1281.4 | 9257.1 | 14 | 0.99×10^{-2} |
| 1Br-2PACz | 1428.0 | 9605.9 | 14 | 1.06×10^{-2} |
| 1I-2PACz | 1383.4 | 10396.8 | 14 | 0.95×10^{-2} |
| 1CF ₃ -2PACz | 1359.6 | 9459.2 | 14 | 1.03×10^{-2} |

For 1CF₃-2PACz, we only calculated the C 1s core-level peak area in the region between 288 and 282 eV. Therefore, the C 1s peak area was divided by 14, excluding the carbon atom in CF₃ group.

Table S2. Summary of optical parameters of 1F-, 1Cl-, 1Br-, 1I-, and 1CF₃-2PACz from **Figure 3B**.

| | 1F-2PACz | 1Cl-2PACz | 1Br-2PACz | 1I-2PACz | 1CF ₃ -2PACz |
|--|--------------------|--------------------|--------------------|--------------------|-------------------------|
| λ_{\max} (nm) | 353 | 352 | 352 | 353 | 342 |
| ϵ (M ⁻¹ cm ⁻¹) | 4.42×10^3 | 3.81×10^3 | 3.59×10^3 | 3.32×10^3 | 2.82×10^3 |
| λ_{onset} (nm) | 367 | 365 | 365 | 366 | 355 |
| $E_{g, \text{opt}}$ (eV) | 3.38 | 3.40 | 3.40 | 3.39 | 3.49 |

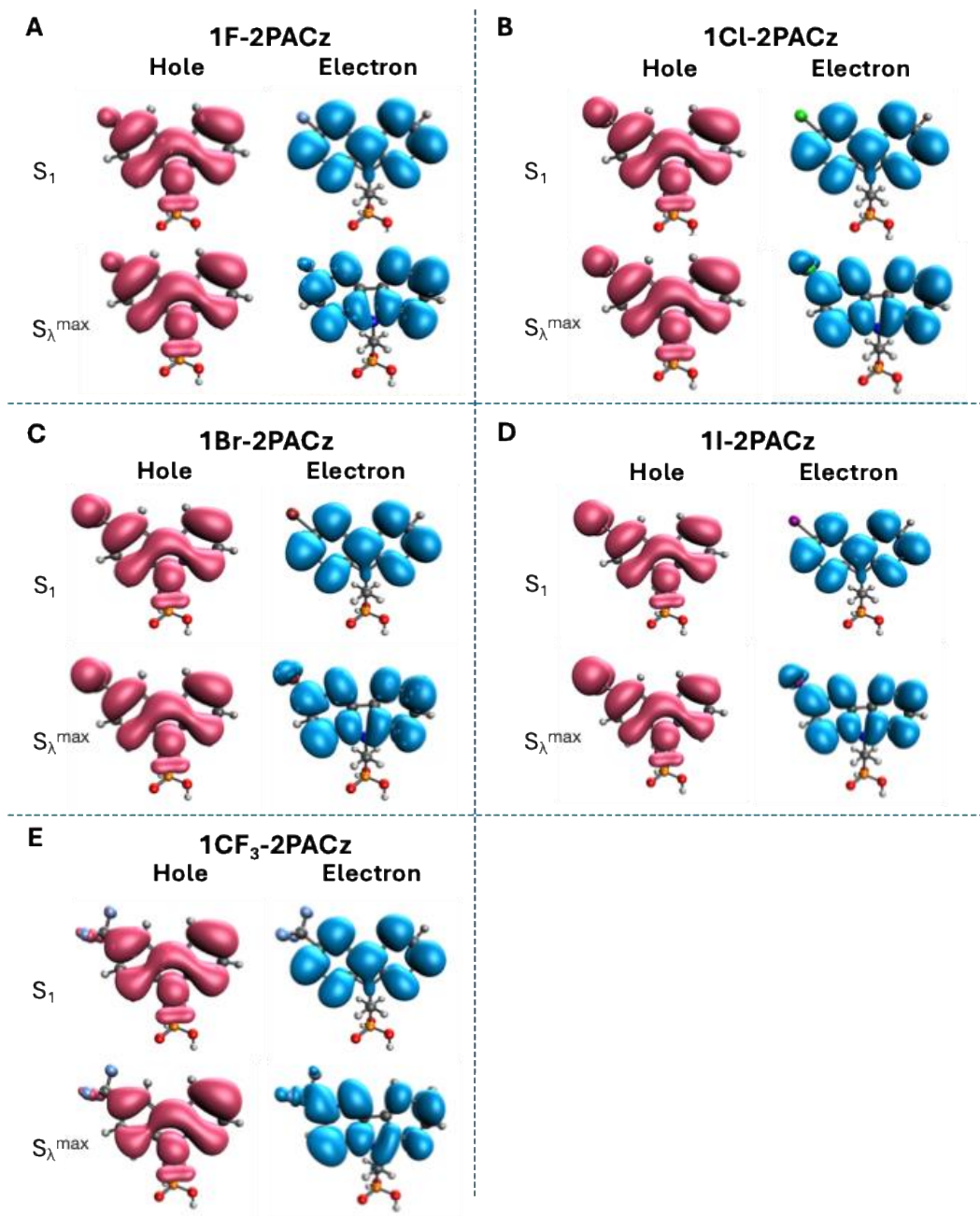


Figure S4. Hole and electron DFT density plots (isovalue = 0.05) of the first excited state (S_1) and the most intense one (S_{λ}^{\max}) of (A) 1F-2PACz, (B) 1Cl-2PACz, (C) 1Br-2PACz, (D) 1I-2PACz, and (E) 1CF₃-2PACz in ethanol.

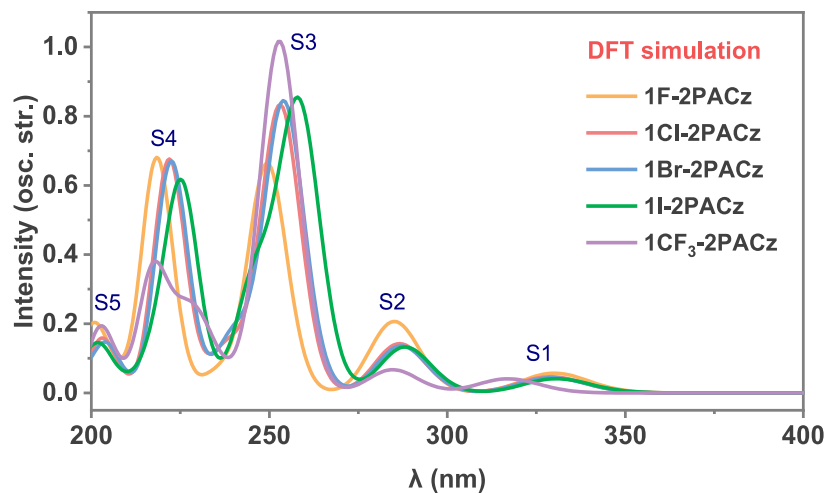


Figure S5. TD-DFT electronic spectra of 1F-, 1Cl-, 1Br-, 1I-, and 1CF₃-2PACz in ethanol. Electronic excitations convoluted with Gaussian functions of 0.25 eV of full width at half maximum.

Table S3. DFT energy and intensity (oscillator strength) of the first 5 excited states of 1F-, 1Cl-, 1Br-, 1I-, and 1CF₃-2PACz in ethanol, and compared with maximum absorption wavelength in measured UV-vis absorption spectra.

| SAMs | Exp. | S1 | | S2 | | S3 | | S4 | | S5 | |
|-------------------------|--------|--------|-----------|--------|-----------|--------|-----------|--------|-----------|--------|-----------|
| | λ (nm) | λ (nm) | Intensity | λ (nm) | Intensity | λ (nm) | Intensity | λ (nm) | Intensity | λ (nm) | Intensity |
| 1F-2PACz | 353 | 330.3 | 0.06 | 285.3 | 0.21 | 249.6 | 0.66 | 237.7 | 0.02 | 235.7 | 0.04 |
| 1Cl-2PACz | 352 | 329.3 | 0.05 | 286.8 | 0.14 | 253.2 | 0.83 | 240.6 | 0.02 | 238.5 | 0.12 |
| 1Br-2PACz | 352 | 329.6 | 0.04 | 287.3 | 0.14 | 258.3 | 0.00 | 254.3 | 0.84 | 241.0 | 0.07 |
| 1I-2PACz | 353 | 330.8 | 0.04 | 303.0 | 0.14 | 288.4 | 0.13 | 263.6 | 0.00 | 285.5 | 0.83 |
| 1CF ₃ -2PACz | 342 | 317.3 | 0.02 | 284.9 | 0.07 | 253.1 | 1.00 | 244.2 | 0.05 | 231.9 | 0.14 |

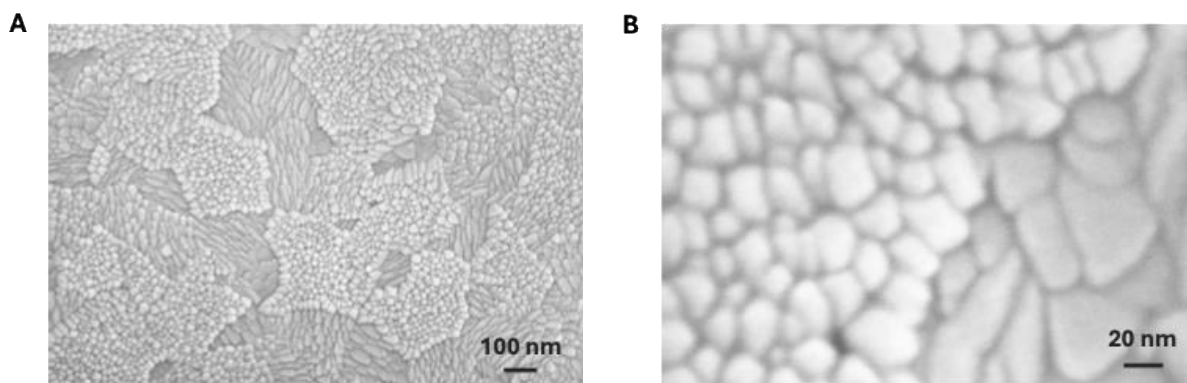


Figure S6. Scanning electron microscope (SEM) images of bare ITO surface with scale bars of (A) 100 nm and (B) 20 nm, respectively.

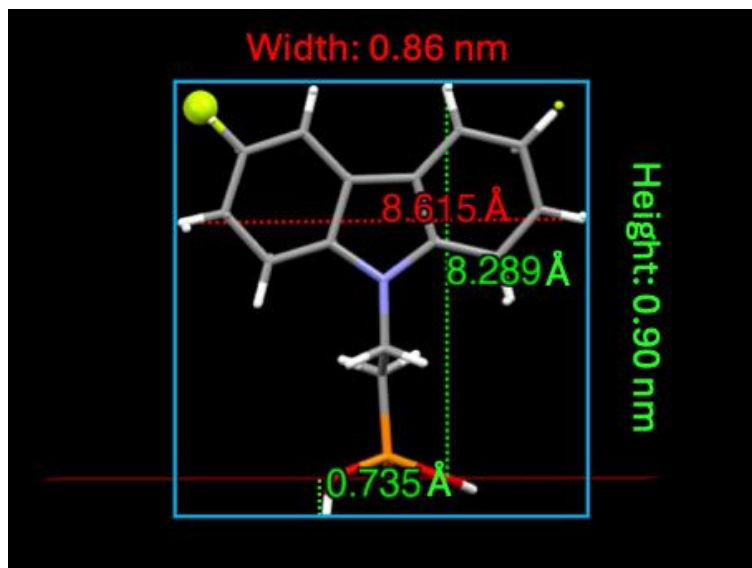


Figure S7. Measured height and width of a single 1F-2PACz molecule as determined from single-crystal X-ray diffraction data.

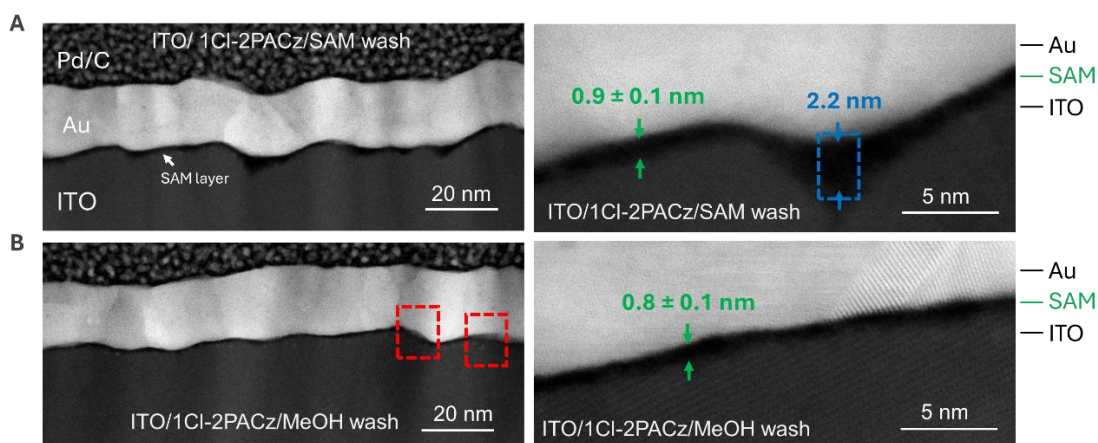


Figure S8. Investigation of thickness and coverage of ITO/1Cl-2PACz layer processed from different methods. SAMs sandwiched between ITO and Au layer. Cross-sectional HAADF-STEM images of (A) ITO/1Cl-2PACz_SAM rinsed and (B) ITO/1Cl-2PACz_MeOH rinsed.

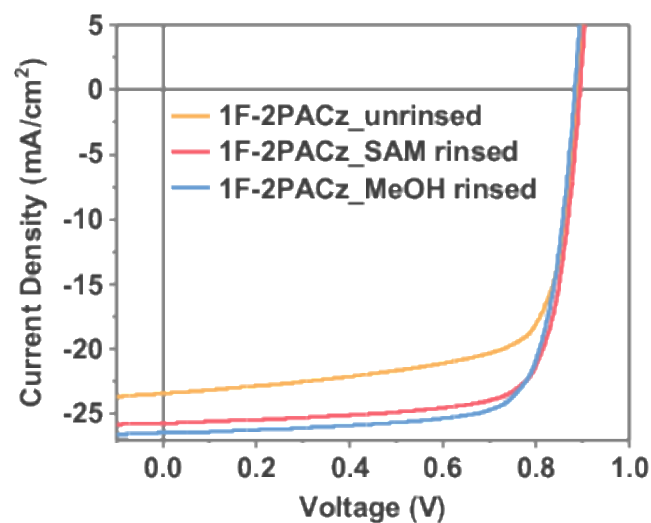


Figure S9. *J-V* characteristics of optimal PM6:L8-BO OSCs with 1F-2PACz prepared via different methods .

Table S4. Photovoltaic parameters of OSCs based on PM6:L8-BO BHJs with 1F-2PACz HTL prepared via different methods measured under illumination with AM 1.5G (100 mW cm⁻²).

| HTLs | V_{oc} [V] | J_{sc} [mA cm ⁻²] | FF [%] | PCE _{max} [%] | R_s [Ω] |
|----------------------|-----------------|------------------------------------|-----------|---------------------------|--------------|
| 1F-2PACz_unrinsed | 0.889 | 23.42 | 71.3 | 14.86 | 99.7 |
| 1F-2PACz_SAM rinsed | 0.894 | 25.72 | 76.6 | 17.62 | 96.2 |
| 1F-2PACz_MeOH rinsed | 0.883 | 26.46 | 76.0 | 17.77 | 97.4 |

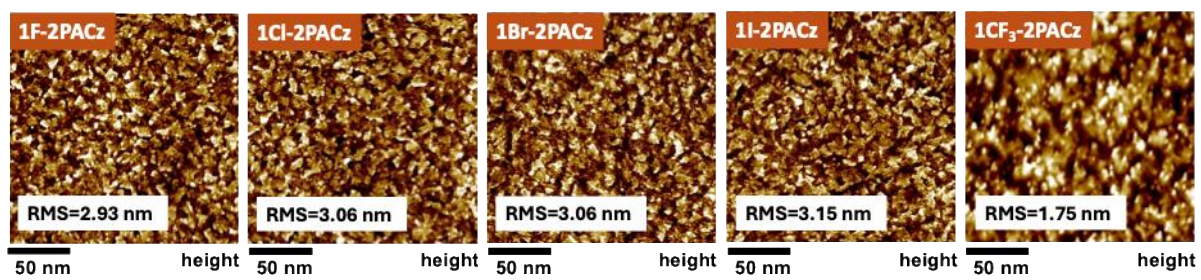


Figure S10. AFM height images for SAMs-modified ITO.

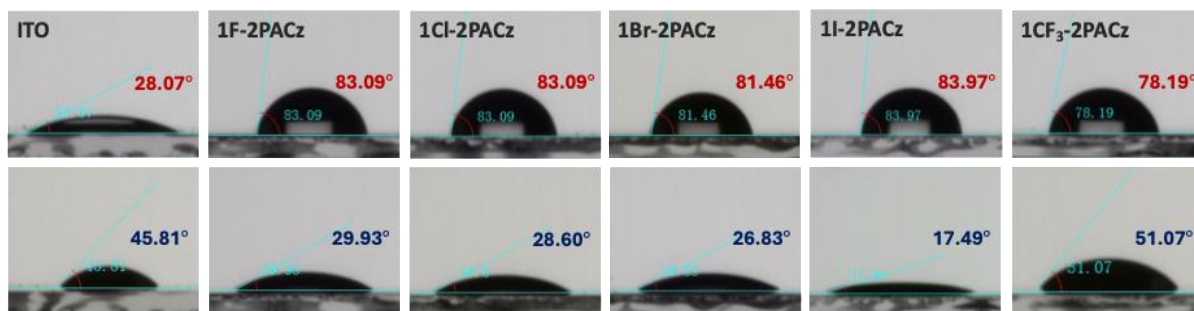


Figure S11. Contact angle images of water (top) and DIM (bottom) on ITO and SAMs-modified ITO.

Table S5. Polarity and dispersion force parameters of H₂O and DIM.

| Liquid | γ_l^p | γ_l^D | γ_l | γ_l^p / γ_l^D |
|------------------|--------------|--------------|------------|---------------------------|
| H ₂ O | 51 | 21.8 | 72.8 | 2.36 |
| DIM | 2.3 | 48.5 | 50.8 | 0.05 |

Table S6. Parameters of contact angle and surface energy bare ITO and ITO glass with various SAMs.

| ITO glass modified with SAMs | Contact angle (°) | | Surface energy γ (mJ m ⁻²) |
|------------------------------|-------------------|-------|---|
| | H ₂ O | DIM | |
| Bare ITO | 28.07 | 45.81 | 62.82 |
| 1F-2PACz | 83.09 | 29.93 | 44.20 |
| 1Cl-2PACz | 83.09 | 28.60 | 44.74 |
| 1Br-2PACz | 81.46 | 26.83 | 45.42 |
| 1I-2PACz | 83.97 | 17.49 | 48.57 |
| 1CF ₃ -2PACz | 78.19 | 51.07 | 28.78 |

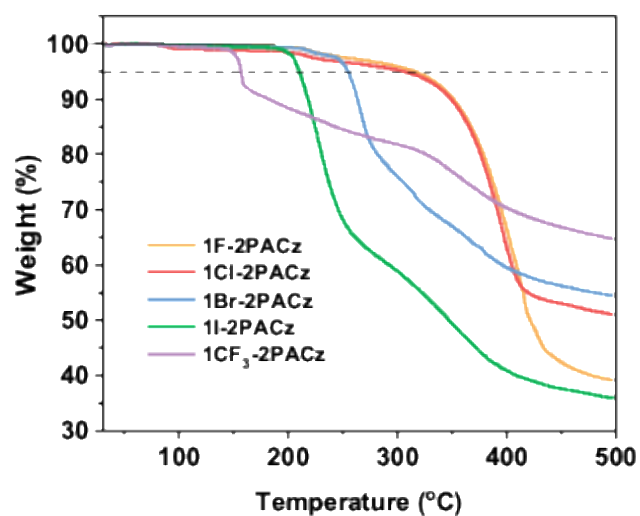


Figure S12. Thermogravimetric analysis (TGA) spectra of 1F-, 1Cl-, 1Br-, 1I-, and 1CF₃-2PACz; heating rate: 10 °C /min, from 30 °C to 500 °C under nitrogen atmosphere.

Table S7. TGA data of 1F-, 1Cl-, 1Br-, 1I-, and 1CF₃-2PACz for 5% weight loss.

| | 1F-2PACz | 1Cl-2PACz | 1Br-2PACz | 1I-2PACz | 1CF ₃ -2PACz |
|--------|----------|-----------|-----------|----------|-------------------------|
| T (°C) | 315 | 305 | 254 | 210 | 156 |

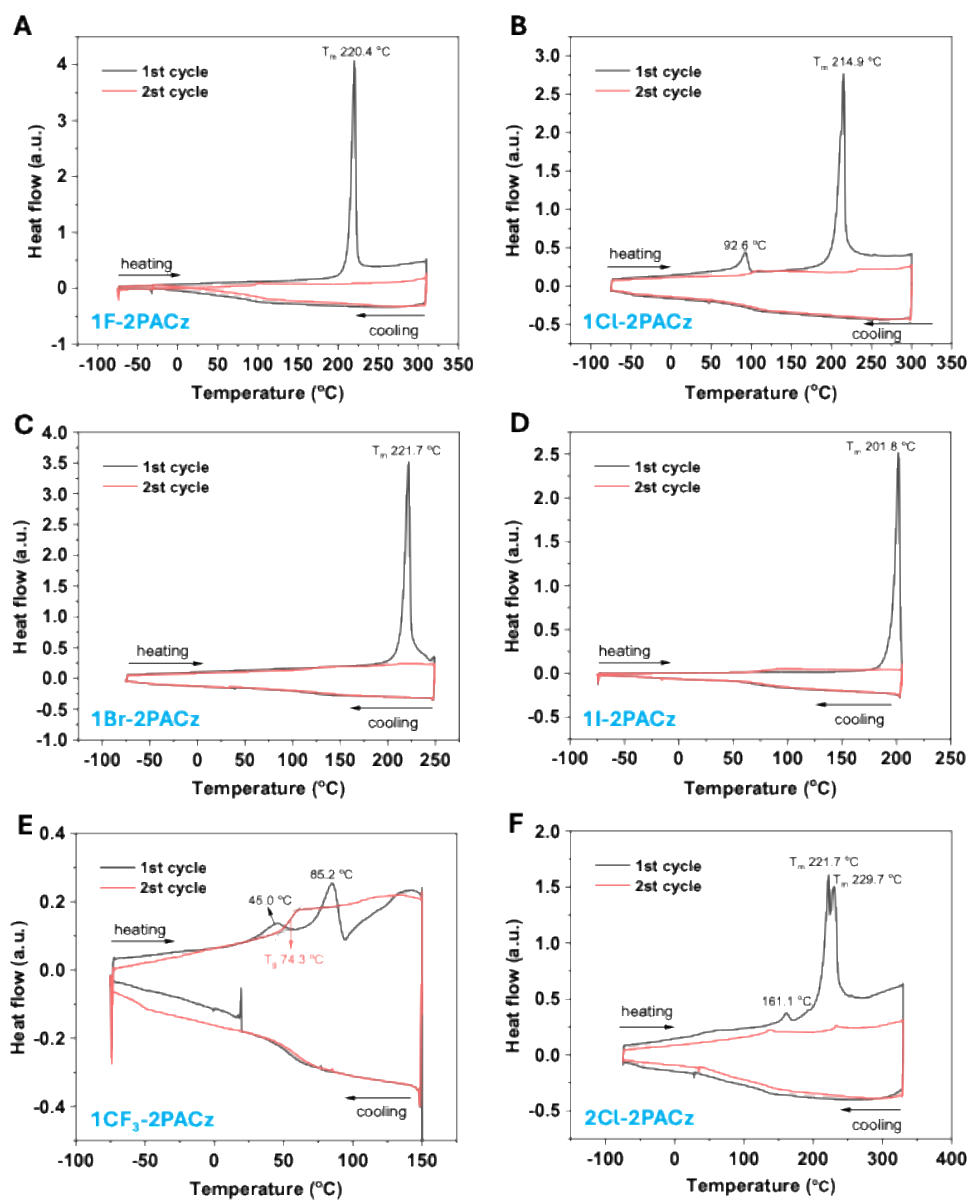


Figure S13. Differential scanning calorimetry (DSC) spectra of SAMs, (A) 1F-2PACz, (B) 1Cl-2PACz, (C) 1Br-2PACz, (D) 1I-2PACz, (E) 1CF₃-2PACz, and (F) 2Cl-2PACz for 2 cycles. Heating/cooling rate: 10 °C/min, under nitrogen atmosphere. (T_m : melting point; T_g : glass transition temperature)

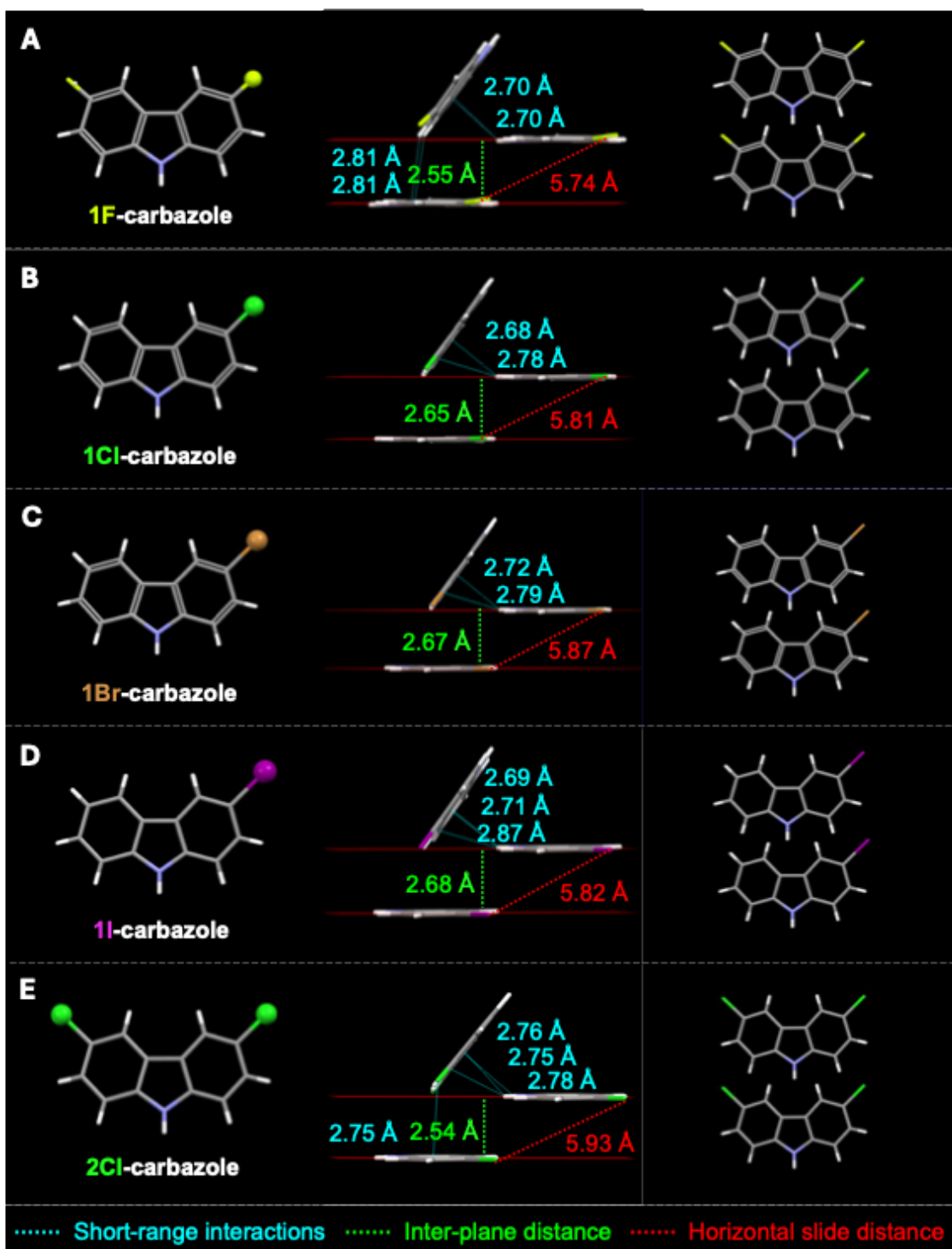


Figure S14. The molecular packing patterns observed in single crystals of monosubstituted pristine carbazole: (A) 1F-carbazole, (B) 1Cl-carbazole, (C) 1Br-carbazole, (D) 1I-carbazole, and (E) 2Cl-carbazole. (1F- (675115), 1Cl- (2303759), 1Br- (279447), and 2Cl-carbazole (2259618) are retrieved from the CCDC database; 1I-carbazole (2440286) is obtained in this paper)

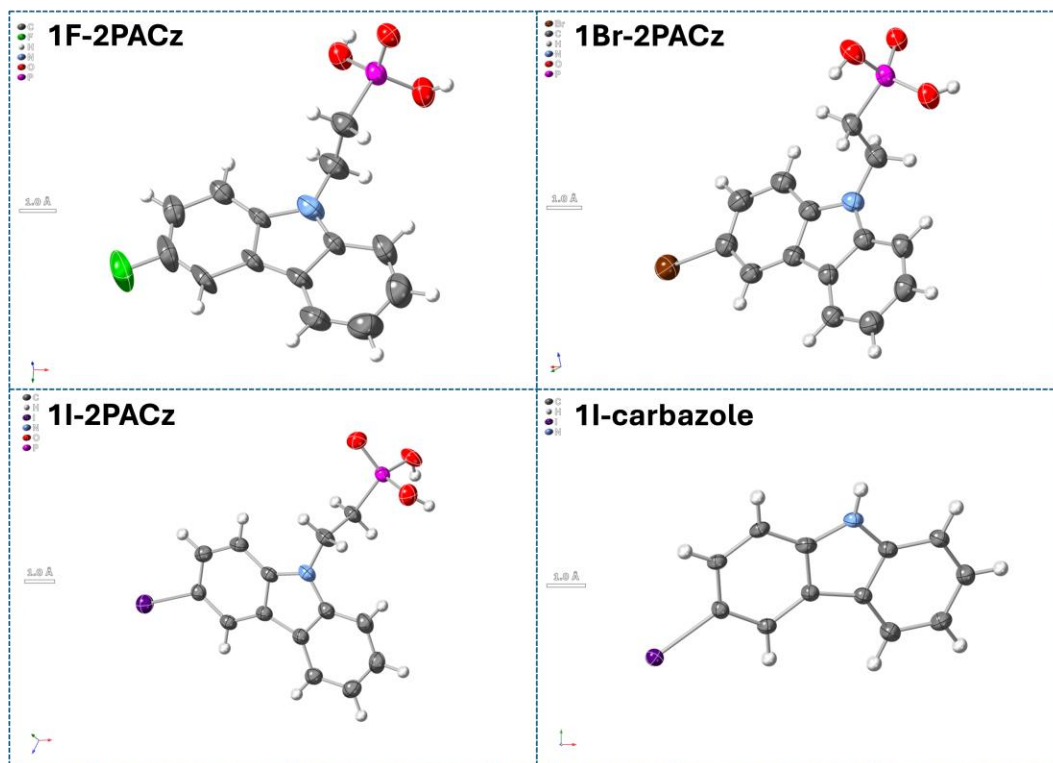


Figure S15. Crystal images of the structures for 1F-2PACz, 1Br-2PACz, 1I-2PACz and 1I-carbazole obtained in this work.

Table S8. Crystallographic information

| | 1F-2PACz | 1Br-2PACz | 1I-carbazole | 1I-2PACz |
|---|--|---|-------------------------------------|---|
| CCDC No. | 2440287 | 2440288 | 2440286 | 2440285 |
| Crystal data | | | | |
| Chemical formula | C ₁₄ H ₁₃ FNO ₃ P | 2(C ₁₄ H ₁₃ BrNO ₃ P)·1.5[C ₂ H ₆ O] | C ₁₂ H ₈ IN | C ₁₄ H ₁₃ INO ₃ P·0.5[C ₂ H ₆ O] |
| M_r | 293.22 | 1130.49 | 293.09 | 424.16 |
| Crystal system, space group | Orthorhombic, <i>Pccn</i> | Monoclinic, <i>P2₁/n</i> | Monoclinic, <i>P2₁/c</i> | Monoclinic, <i>P2₁/n</i> |
| Temperature (K) | 278 | 153 | 102 | 150 |
| a, b, c (Å) | 26.4651 (9), 13.4060 (5), 7.5991 (3) | 21.7792 (6), 4.8213 (2), 43.2639 (13) | 20.9273 (6), 5.8164 (2), 7.9917 (2) | 15.3317 (2), 4.7480 (1), 22.9810 (4) |
| α, β, γ (°) | 90, 90, 90 | 90, 95.607 (3), 90 | 90, 93.079 (3), 90 | 90, 107.568 (2), 90 |
| V (Å³) | 2696.11 (16) | 4521.1 (3) | 971.36 (5) | 1594.87 (5) |
| Z | 8 | 4 | 4 | 4 |
| m (mm⁻¹) | 2.00 | 4.85 | 25.51 | 16.85 |
| Crystal size (mm) | 0.06 × 0.05 × 0.02 | 0.23 × 0.03 × 0.02 | 0.20 × 0.15 × 0.04 | 0.25 × 0.03 × 0.03 |
| Data collection | | | | |
| Diffractometer | XtaLAB Synergy R, HyPix | XtaLAB Synergy R, HyPix | XtaLAB Synergy R, HyPix | XtaLAB Synergy R, HyPix |
| T_{min}, T_{max} | 0.930, 0.999 | 0.715, 1.000 | 0.334, 1.000 | 0.602, 1.000 |
| No. of measured, independent and observed [<i>I</i> > 2σ(<i>I</i>)] reflections | 13407, 2691, 2192 | 44488, 9063, 6001 | 8368, 1899, 1816 | 15620, 3187, 2831 |
| R_{int} | 0.028 | 0.091 | 0.058 | 0.039 |
| (sin θ/λ)_{max} (Å⁻¹) | 0.629 | 0.629 | 0.629 | 0.627 |
| Refinement | | | | |
| R[F² > 2σ(F²)], wR(F²), S | 0.049, 0.133, 1.10 | 0.057, 0.158, 1.01 | 0.045, 0.132, 1.12 | 0.030, 0.081, 1.06 |
| No. of reflections | 2691 | 9063 | 1899 | 3187 |
| No. of parameters | 237 | 555 | 127 | 183 |
| No. of restraints | 41 | 7 | 0 | 0 |
| H-atom treatment | H atoms treated by a | H-atom parameters | H-atom parameters | H-atom parameters |

| | | | | |
|---|---|-------------|-------------|-------------|
| | mixture of independent and constrained refinement | constrained | constrained | constrained |
| $\Delta\rho_{\max}, \Delta\rho_{\min}$ ($e \text{ \AA}^{-3}$) | 0.18, -0.40 | 0.75, -0.72 | 2.15, -1.27 | 0.90, -0.70 |

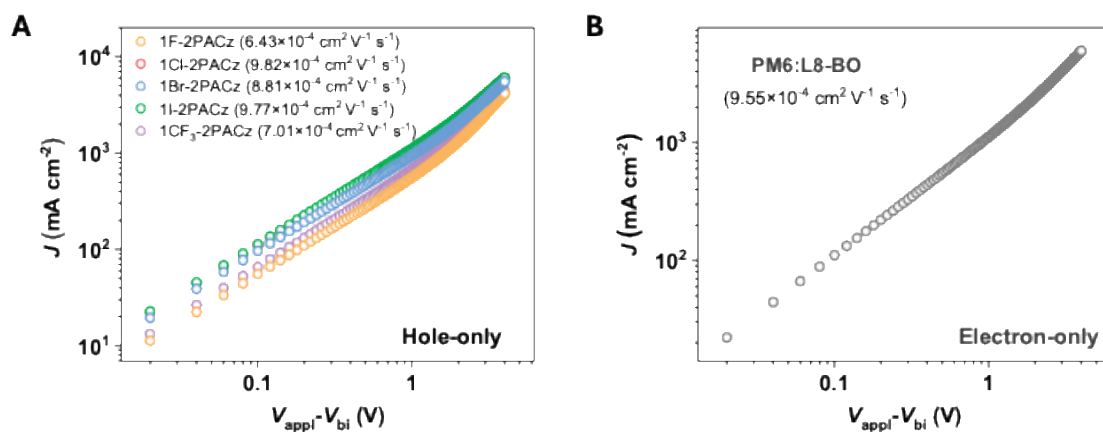


Figure S16. The J dependence on $V_{\text{appl}}-V_{\text{bi}}$ of **(A)** hole-only and **(B)** electron-only devices.

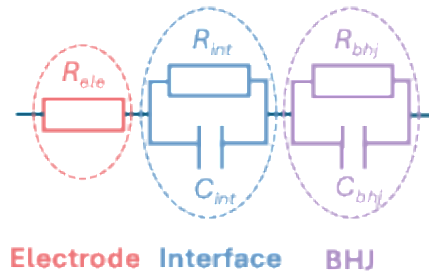


Figure S17. The equivalent-circuit model employed for electrochemical impedance spectroscopy (EIS) fitting of the devices. R_{ele} corresponds to electrode resistance including ITO and Ag; R_{int} and C_{int} parallel connection corresponds to resistance and capacitance of the interface layer; R_{bhj} and C_{bhj} parallel connection corresponds to resistance and capacitance of the BHJ layer.

Table S9. The fitting parameters of OSCs from Nyquist plots.

| Element | Resistance R [Ω] | Capacitance C [F] | Phase angle α |
|-----------|-----------------------------|---------------------|----------------------|
| Electrode | R_{ele} | | |
| Interface | R_{int} | C_{int} | |
| BHJ | R_{bhj} | C_{bhj} | |

| Element | Resistance R [Ω] | Capacitance C [F] | Phase angle α |
|---------|-----------------------------|---------------------|----------------------|
| 1 | | | |
| F 2 | | | |
| - 4 | | | |
| 2 5 | | | |
| P 4 | 1.09 | | 29.87 |
| A . 8 | | | 6.90 |
| C 2 | | | |
| z | | | |
| 1 2 | | | |
| C 0 | | | |
| 1 7 | 1.13 | | 27.60 |
| - 5 | | | 1.16 |
| 2 5 | | | |

| | | | |
|---------|------|-------|------|
| P . | | | |
| A 7 | | | |
| C | | | |
| z | | | |
| 1 | | | |
| B | | | |
| r 2 | | | |
| 1 2 | | | |
| - 1 8 2 | | | |
| 2 5 0 | 12.5 | 31.91 | 6.76 |
| P 7 . 7 | | | |
| A . 1 3 | | | |
| C 2 7 | | | |
| z | | | |
| 1 | | | |
| I 2 | | | |
| - 2 2 | | | |
| 2 2 7 2 | 15.4 | 38.76 | 5.3 |
| P 8 . 5 | | | |
| A . 8 9 | | | |
| C 9 5 | | | |
| z | | | |
| 1 | | | |
| C | | | |
| F 2 | | | |
| 3 6 2 | | | |
| - 2 8 2 | | | |
| 2 9 . 5 | 9.4 | 16.82 | 17.6 |
| P . 7 4 | | | |
| A 6 6 | | | |
| C | | | |
| z | | | |

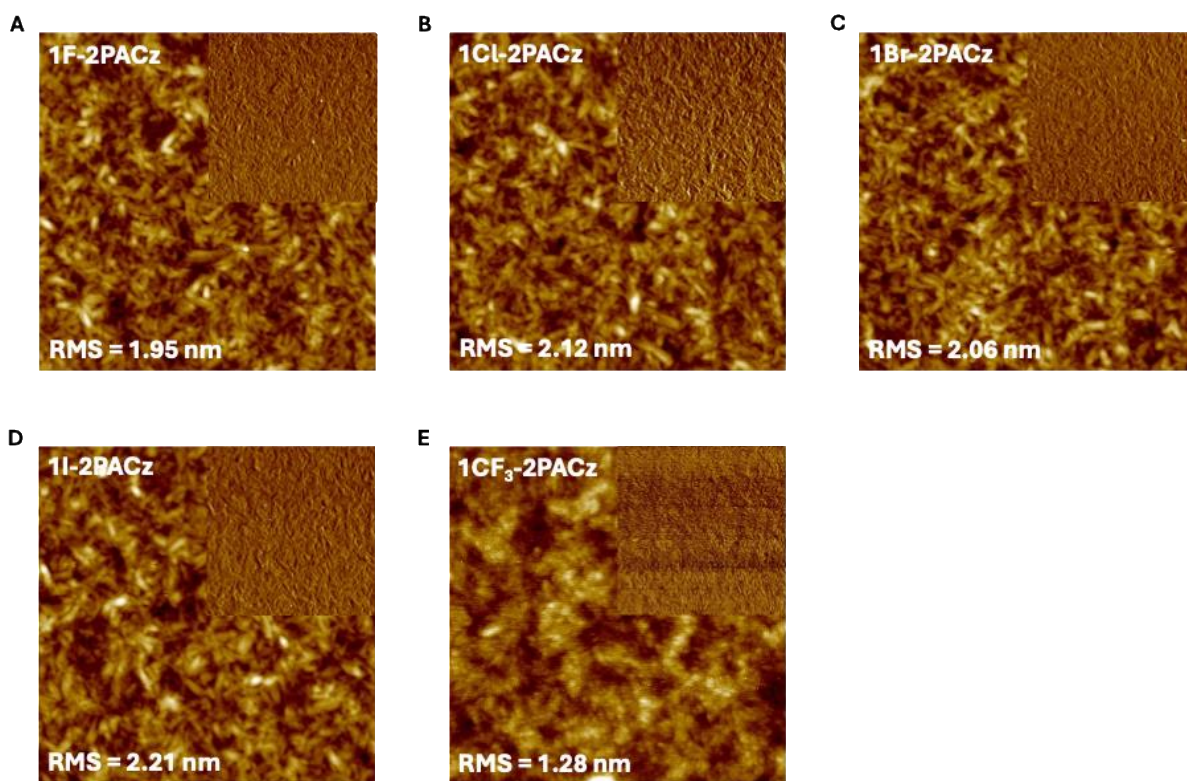


Figure S18. Atomic force microscopy (AFM) height and phase (inset) images for the PM6:L8-BO blends on (A) ITO/1F-PACz, (B) ITO/1Cl-2PACz, (C) ITO/1Br-2PACz, (D) ITO/1I-2PACz, and (E) ITO/1CF₃-2PACz. Scale: $2 \times 2 \mu\text{m}^2$.

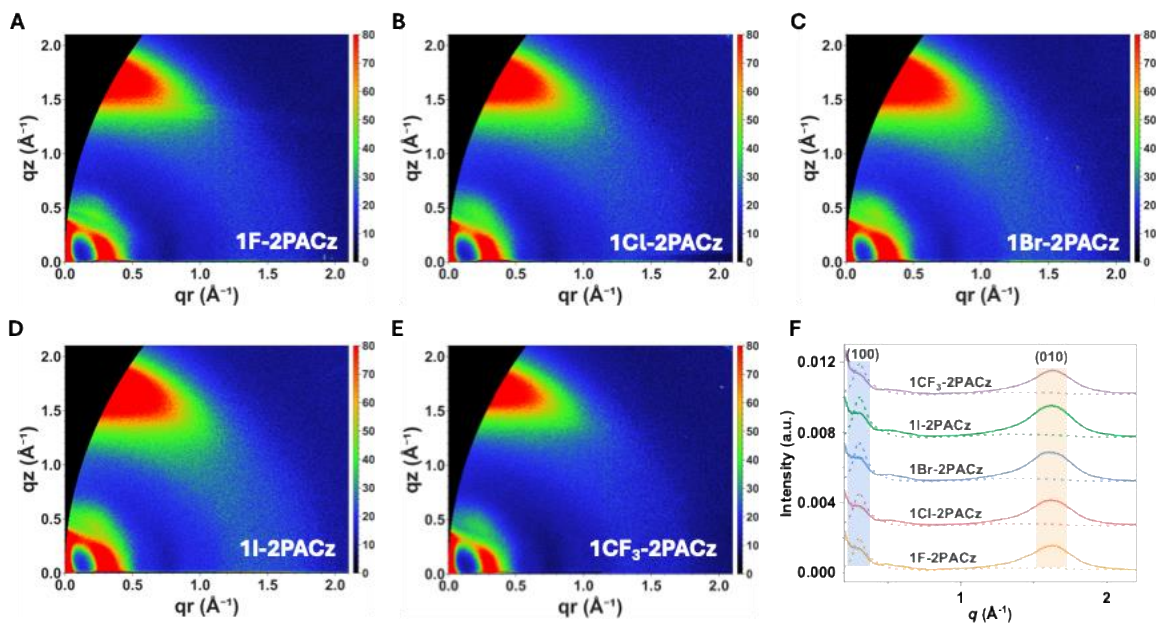


Figure S19. Two-dimensional grazing-incidence wide-angle X-ray scattering (GIWAXS) patterns for the PM6:L8-BO blends on (A) ITO/1F-2PACz, (B) ITO/1Cl-2PACz, (C) ITO/1Br-2PACz, (D) ITO/1I-2PACz, and (E) ITO/1CF₃-2PACz. (F) The out-of-plane (OOP) and in-plane (IP) line cut profiles of the 2D GIWAXS of PM6:L8-BO blends based on different SAM layer (the solid lines represent the OOP direction and the dashed lines represent the IP direction).

Table S10. The detailed GIWAX data of OOP direction for blend PM6:L8-BO films on different HTLs.

| HTLs | (010) peaks | | | |
|-------------------------|------------------------------|-------------------------------|-------------------------------|-------------------------|
| | q (\AA^{-1}) | d-spacing (\AA) | FWHM (\AA^{-1}) | CCL (\AA) |
| 1F-2PACz | 1.61 | 3.86 | 0.395 | 14.30 |
| 1Cl-2PACz | 1.61 | 3.89 | 0.401 | 14.08 |
| 1Br-2PACz | 1.60 | 3.93 | 0.398 | 14.21 |
| 1I-2PACz | 1.63 | 3.87 | 0.397 | 14.24 |
| 1CF ₃ -2PACz | 1.62 | 3.87 | 0.379 | 14.93 |

Table S11. The detailed GIWAX data of IP direction for blend PM6:L8-BO films on different HTLs.

| HTLs | (100) peaks | | | |
|-------------------------|------------------------------|-------------------------------|-------------------------------|-------------------------|
| | q (\AA^{-1}) | d-spacing (\AA) | FWHM (\AA^{-1}) | CCL (\AA) |
| 1F-2PACz | 0.30 | 20.69 | 0.105 | 54.11 |
| 1Cl-2PACz | 0.31 | 20.43 | 0.115 | 49.34 |
| 1Br-2PACz | 0.31 | 20.18 | 0.115 | 49.13 |
| 1I-2PACz | 0.30 | 20.69 | 0.118 | 48.13 |
| 1CF ₃ -2PACz | 0.31 | 20.43 | 0.114 | 49.82 |

4. Nuclear Magnetic Resonance (NMR) Spectra

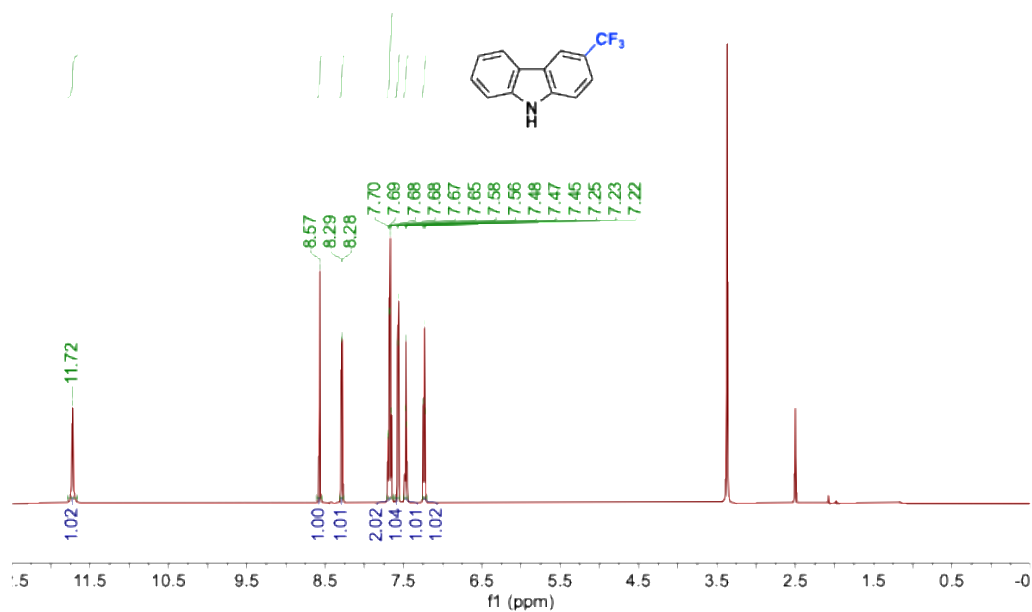


Figure S20. ^1H NMR spectrum (600 MHz) for **1-CF₃** taken in DMSO-*d*₆ at 25 °C.

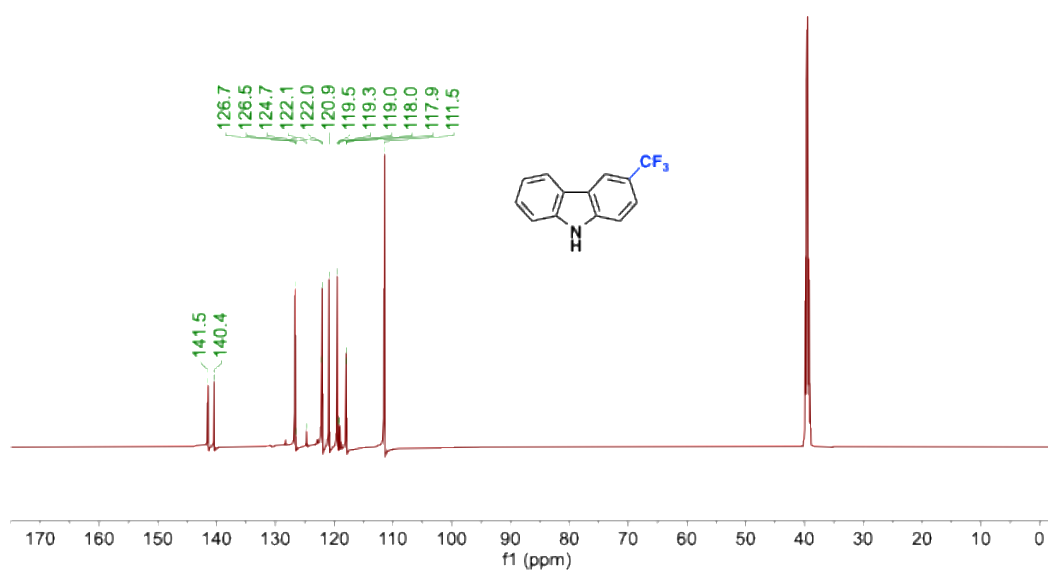


Figure S21. ^{13}C NMR spectrum (150 MHz) for **1-CF₃** taken in DMSO-*d*₆ at 25 °C.

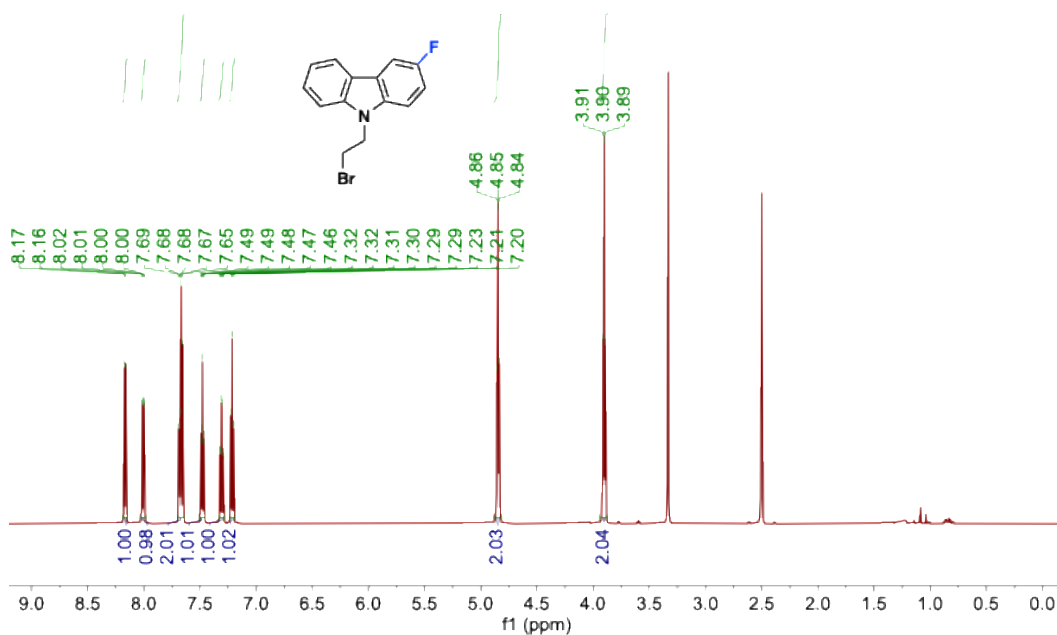


Figure S22. ^1H NMR spectrum (600 MHz) for **2-F** taken in $\text{DMSO-}d_6$ at 25 °C.

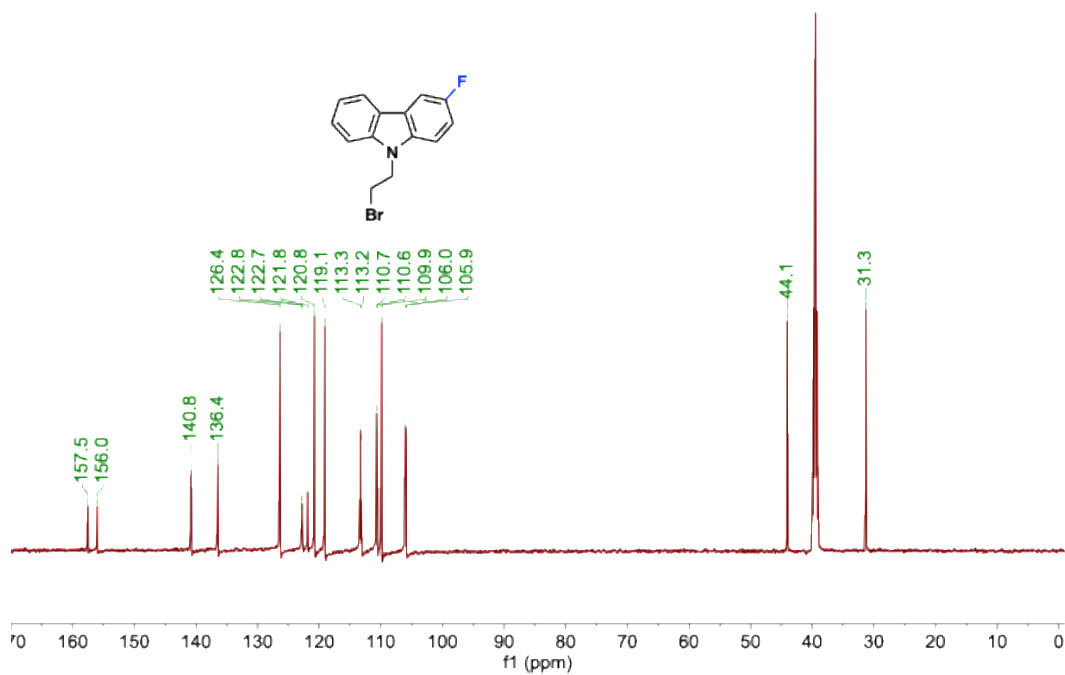


Figure S23. ^{13}C NMR spectrum (150 MHz) for **2-F** taken in $\text{DMSO-}d_6$ at 25 °C.

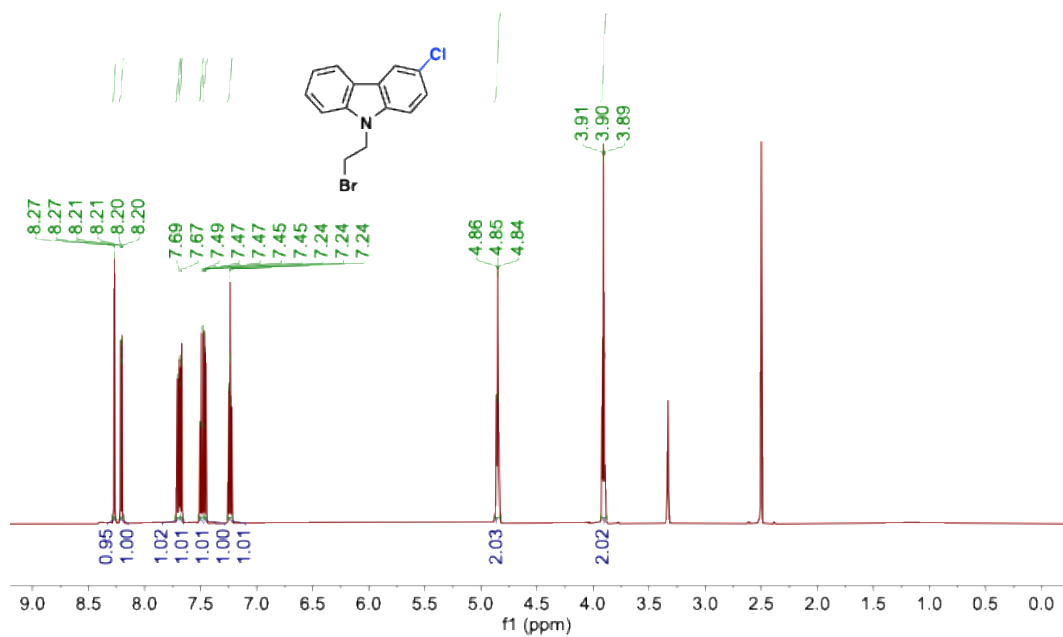


Figure S24. ^1H NMR spectrum (600 MHz) for **2-Cl** taken in $\text{DMSO-}d_6$ at 25 °C.

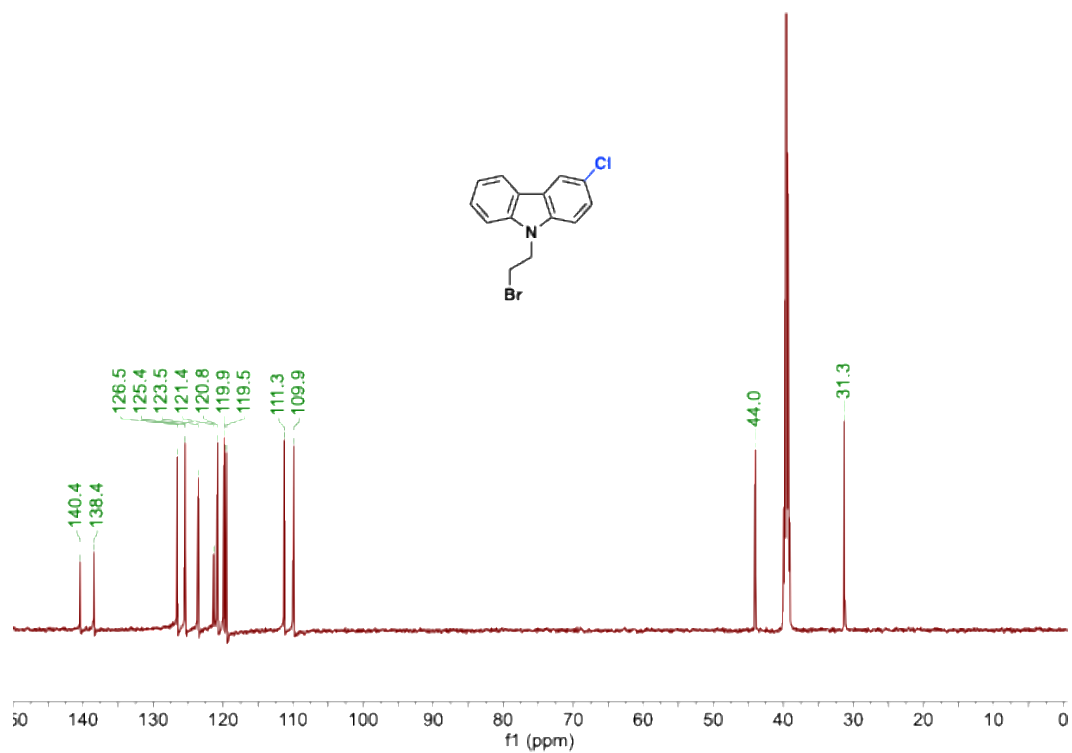


Figure S25. ^{13}C NMR spectrum (150 MHz) for **2-Cl** taken in $\text{DMSO-}d_6$ at 25 °C.

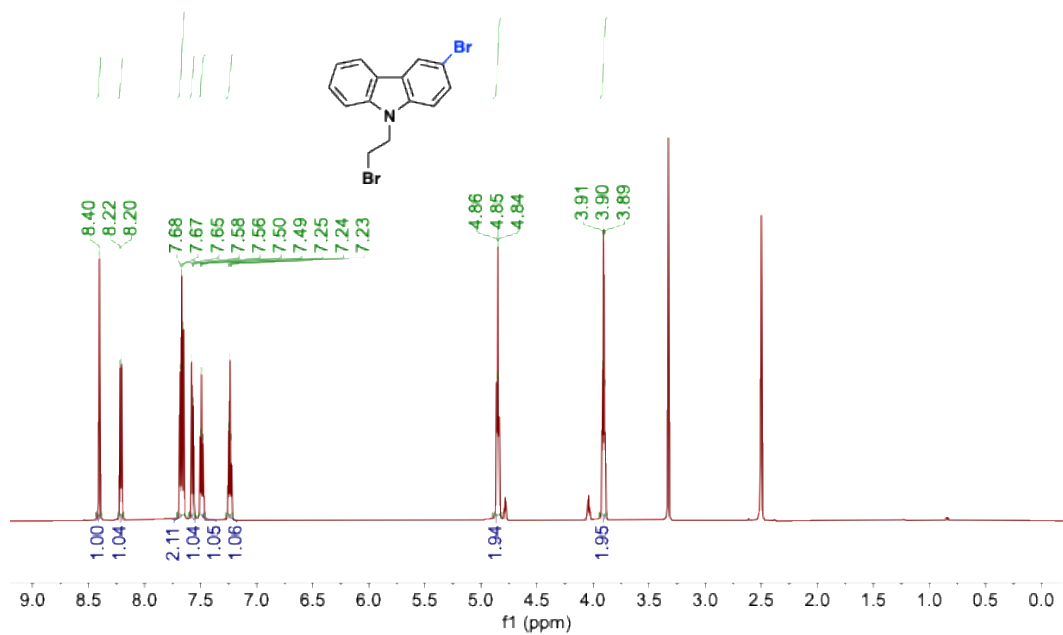


Figure S26. ^1H NMR spectrum (600 MHz) for **2-Br** taken in $\text{DMSO-}d_6$ at 25 °C.

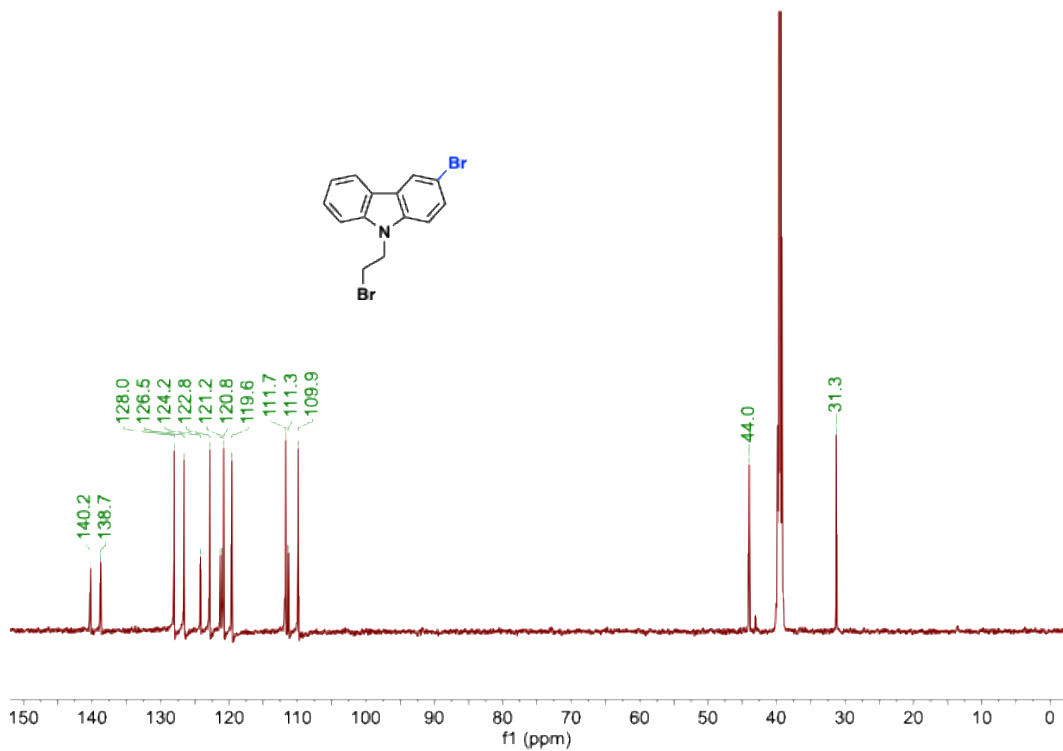


Figure S27. ^{13}C NMR spectrum (150 MHz) for **2-Br** taken in $\text{DMSO-}d_6$ at 25 °C.

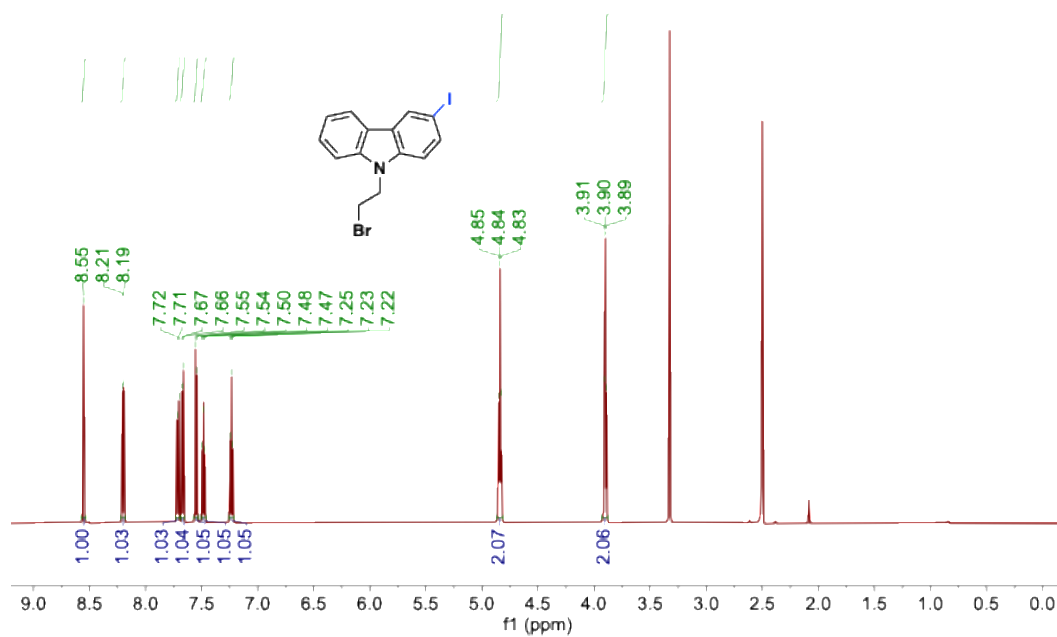


Figure S28. ^1H NMR spectrum (600 MHz) for **2-I** taken in $\text{DMSO-}d_6$ at 25 °C.

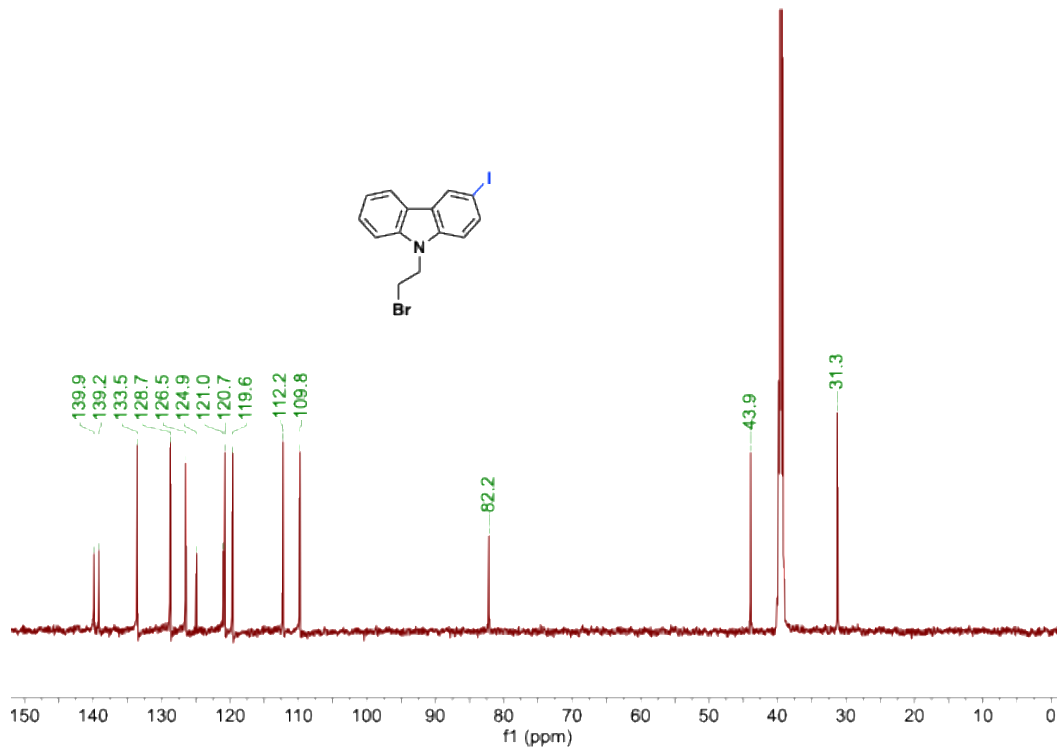


Figure S29. ^{13}C NMR spectrum (150 MHz) for **2-I** taken in $\text{DMSO-}d_6$ at 25 °C.

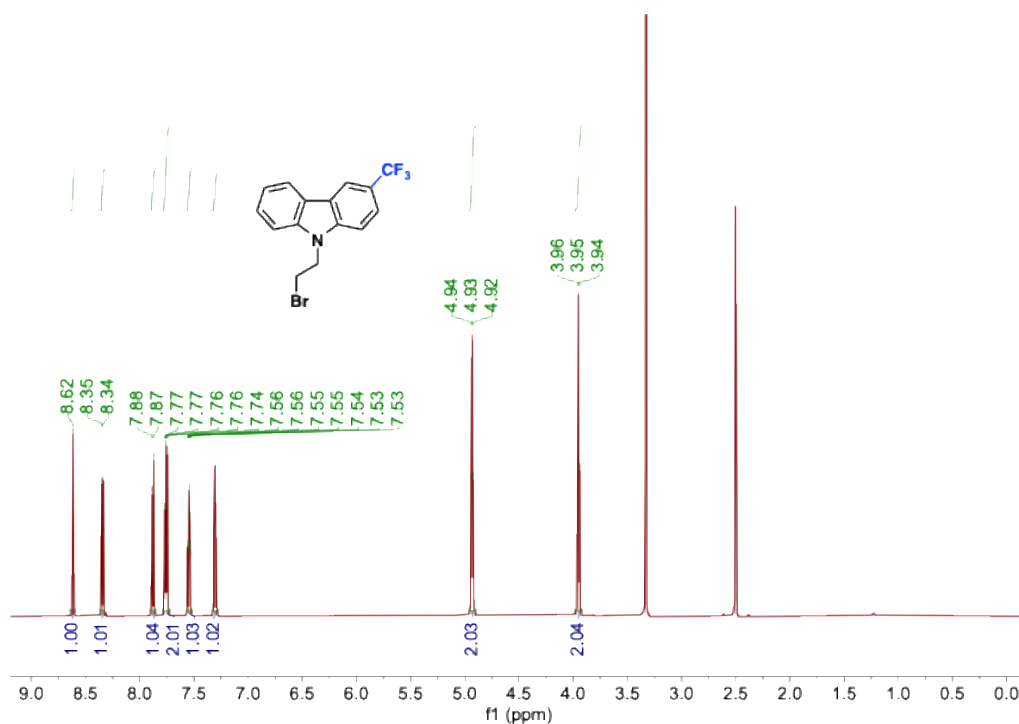


Figure S30. ^1H NMR spectrum (600 MHz) for **2-CF₃** taken in DMSO-*d*₆ at 25 °C.

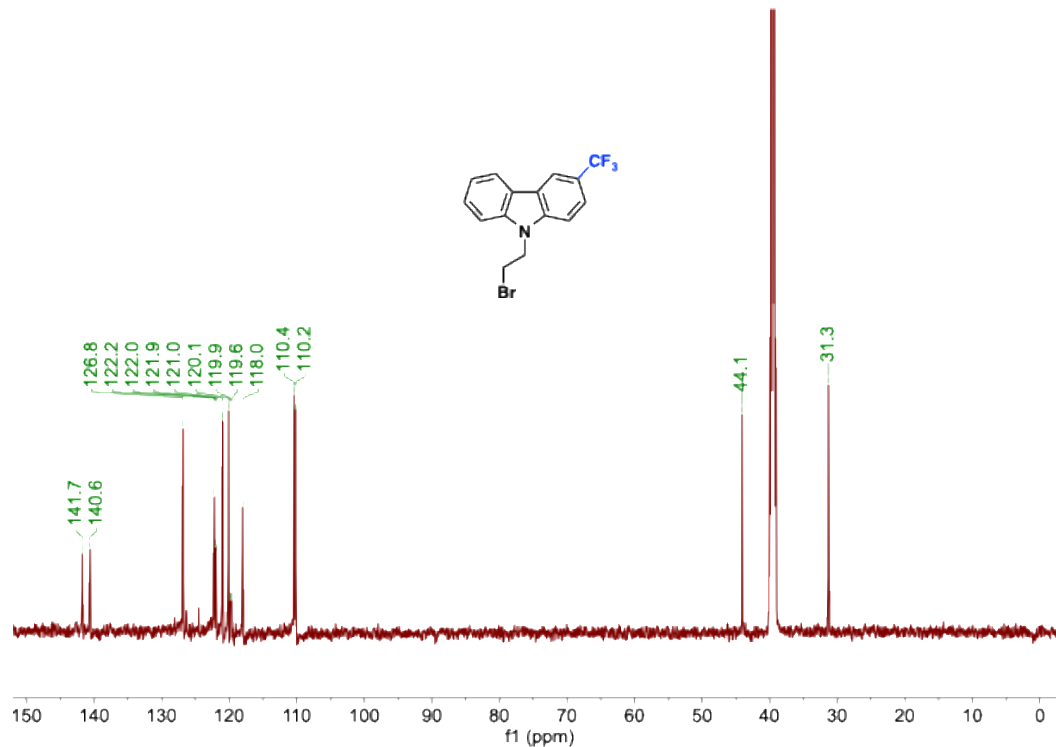


Figure S31. ^{13}C NMR spectrum (150 MHz) for **2-CF₃** taken in DMSO-*d*₆ at 25 °C.

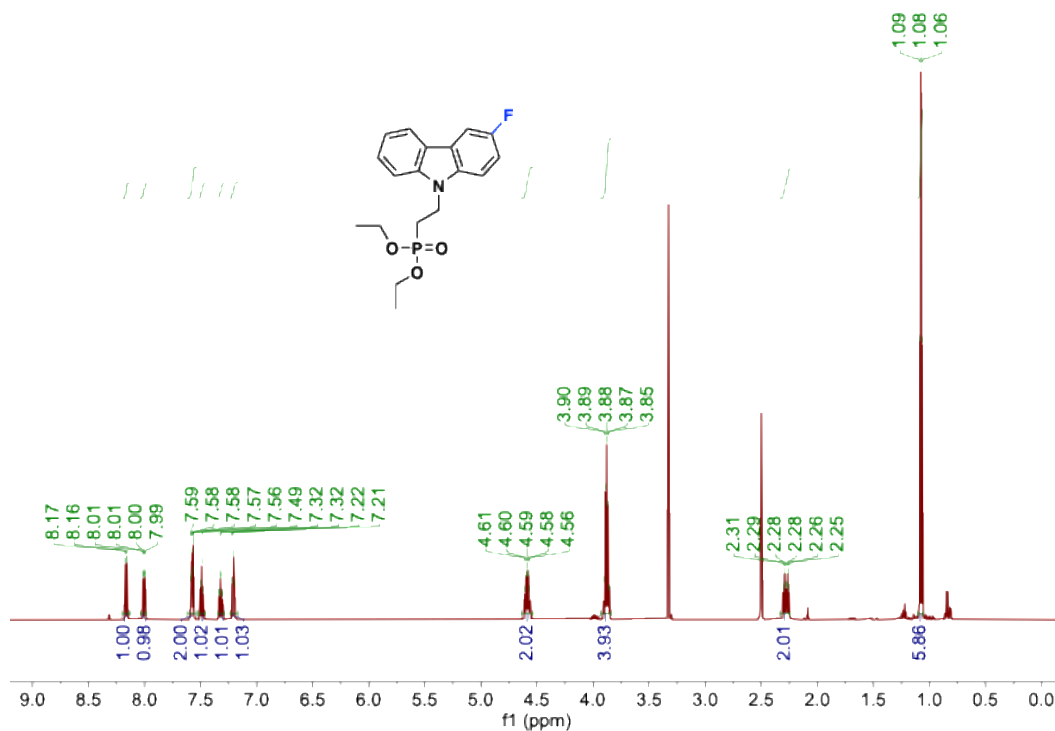


Figure S32. ^1H NMR spectrum (600 MHz) for **3-F** taken in $\text{DMSO-}d_6$ at $25\text{ }^\circ\text{C}$.

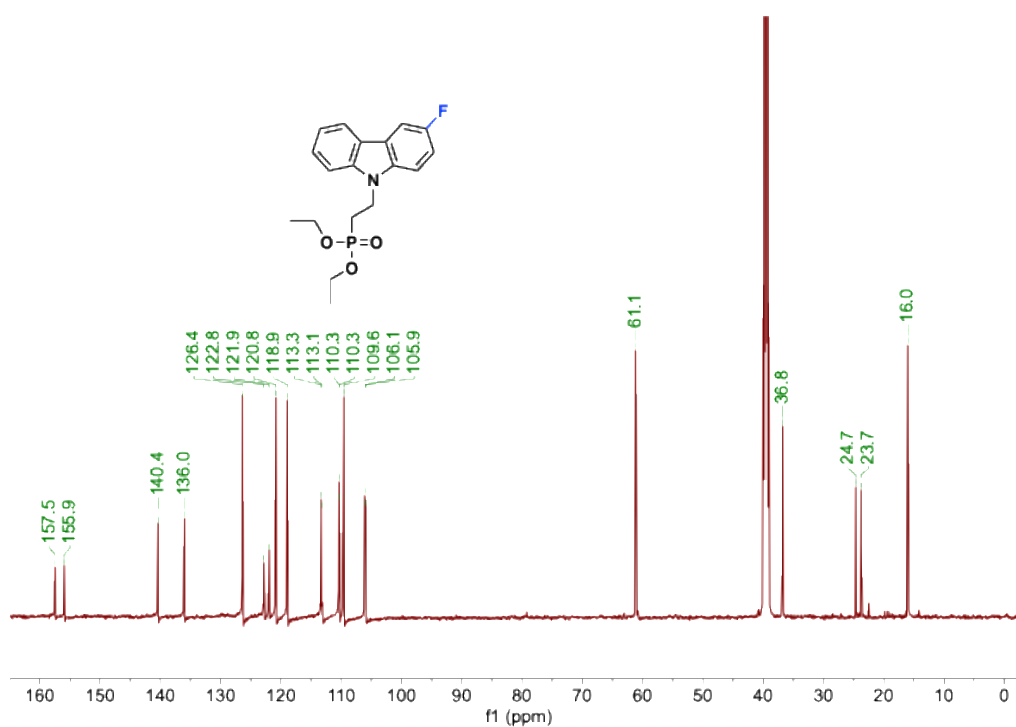


Figure S33. ^{13}C NMR spectrum (150 MHz) for **3-F** taken in $\text{DMSO-}d_6$ at $25\text{ }^\circ\text{C}$.

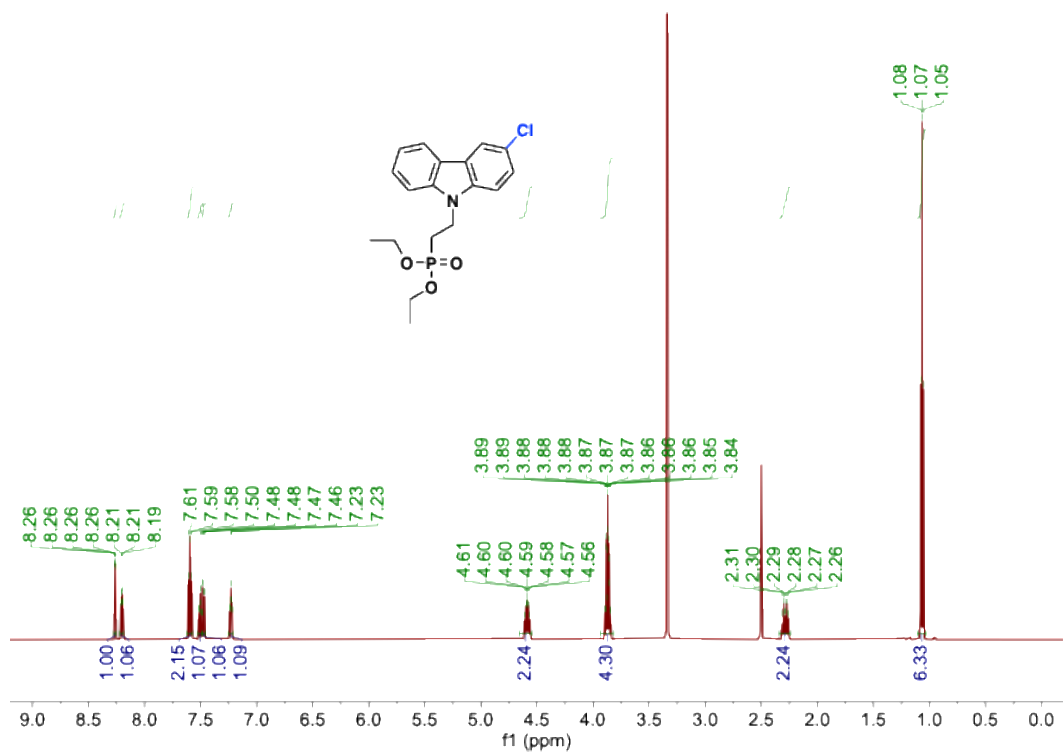


Figure S34. ^1H NMR spectrum (600 MHz) for **3-Cl** taken in $\text{DMSO-}d_6$ at 25 °C.

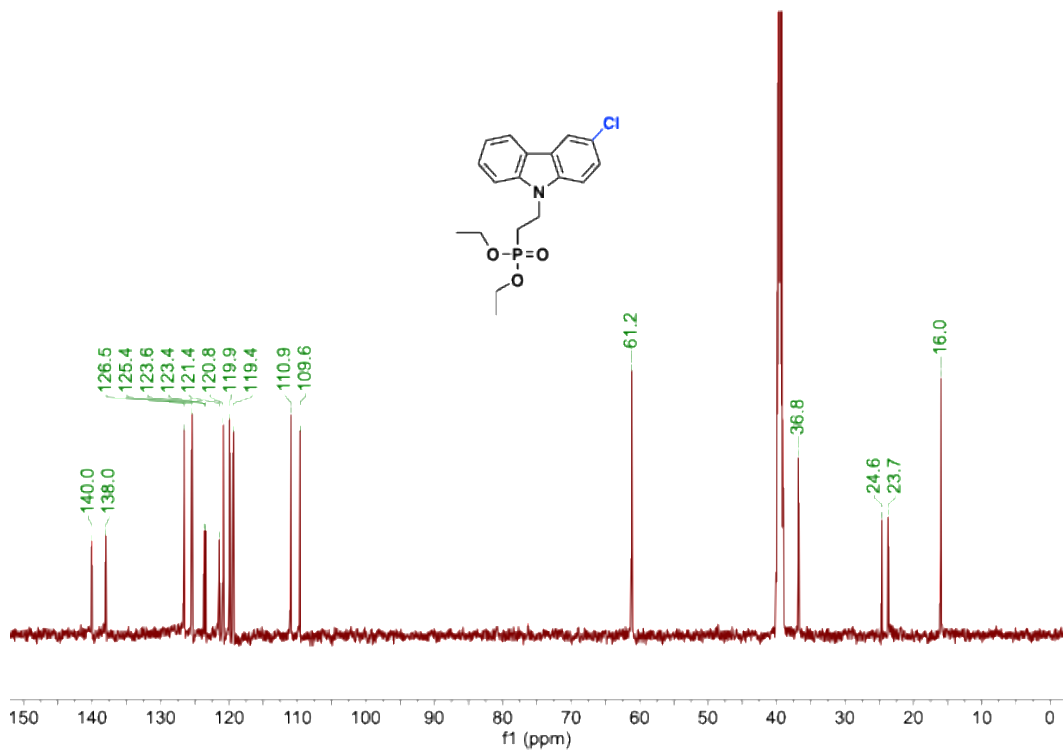


Figure S35. ^{13}C NMR spectrum (150 MHz) for **3-Cl** taken in $\text{DMSO-}d_6$ at 25 °C.

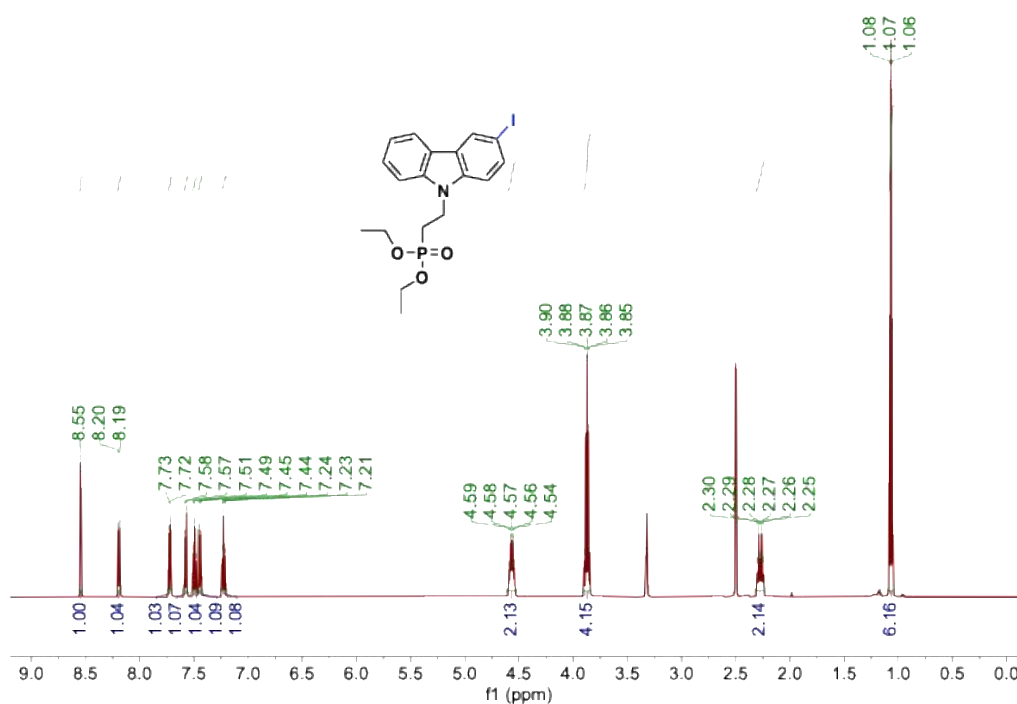


Figure S36. ^1H NMR spectrum (600 MHz) for **3-I** taken in $\text{DMSO-}d_6$ at 25 °C.

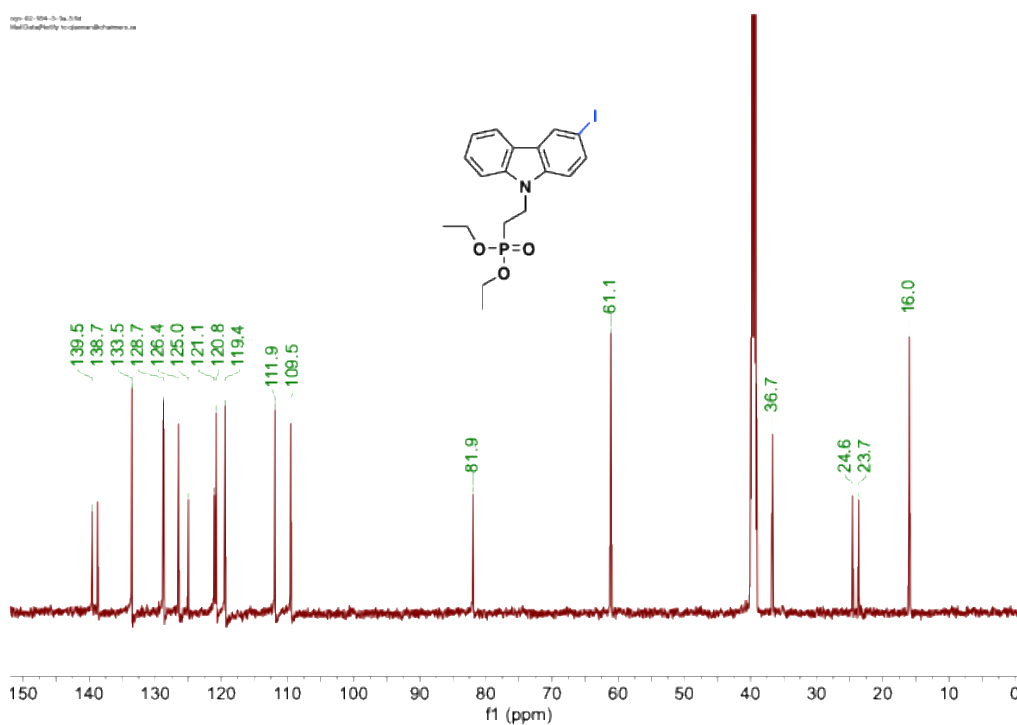


Figure S37. ^{13}C NMR spectrum (150 MHz) for **3-I** taken in $\text{DMSO-}d_6$ at 25 °C.

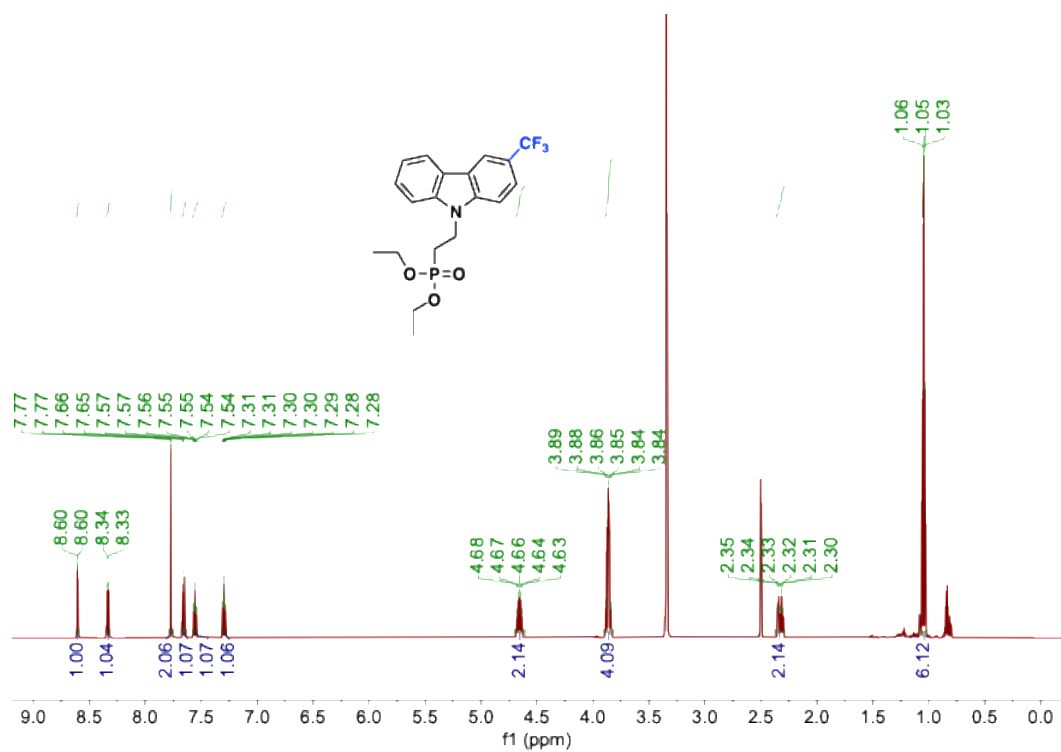


Figure S38. ¹H NMR spectrum (600 MHz) for 3-CF₃ taken in DMSO-*d*₆ at 25 °C.

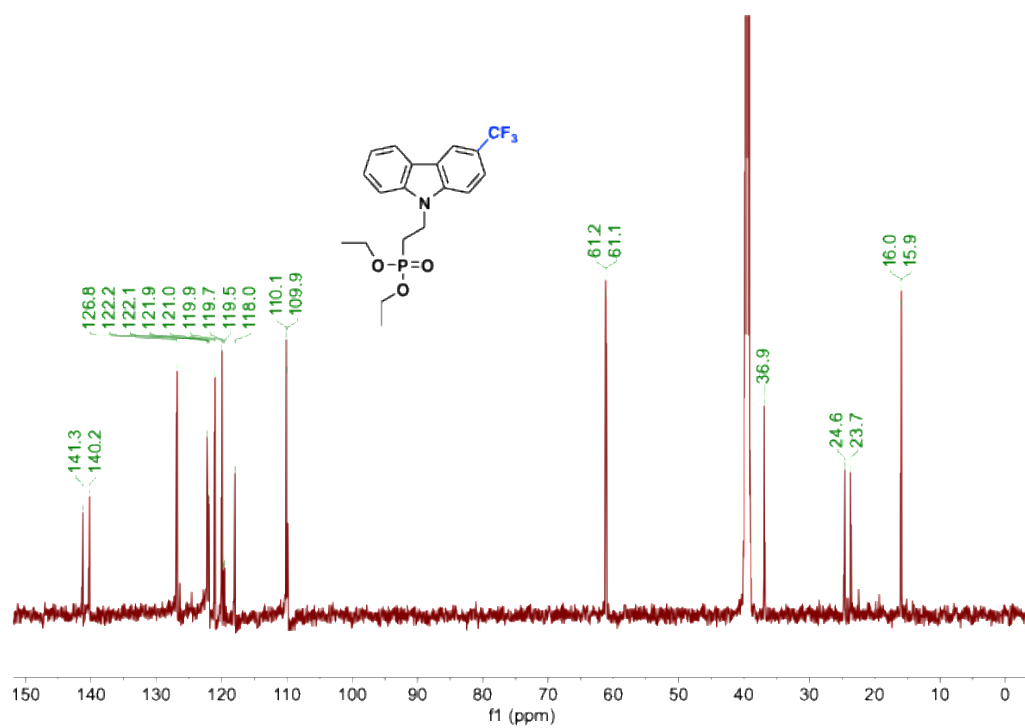


Figure S39. ¹³C NMR spectrum (150 MHz) for 3-CF₃ taken in DMSO-*d*₆ at 25 °C.

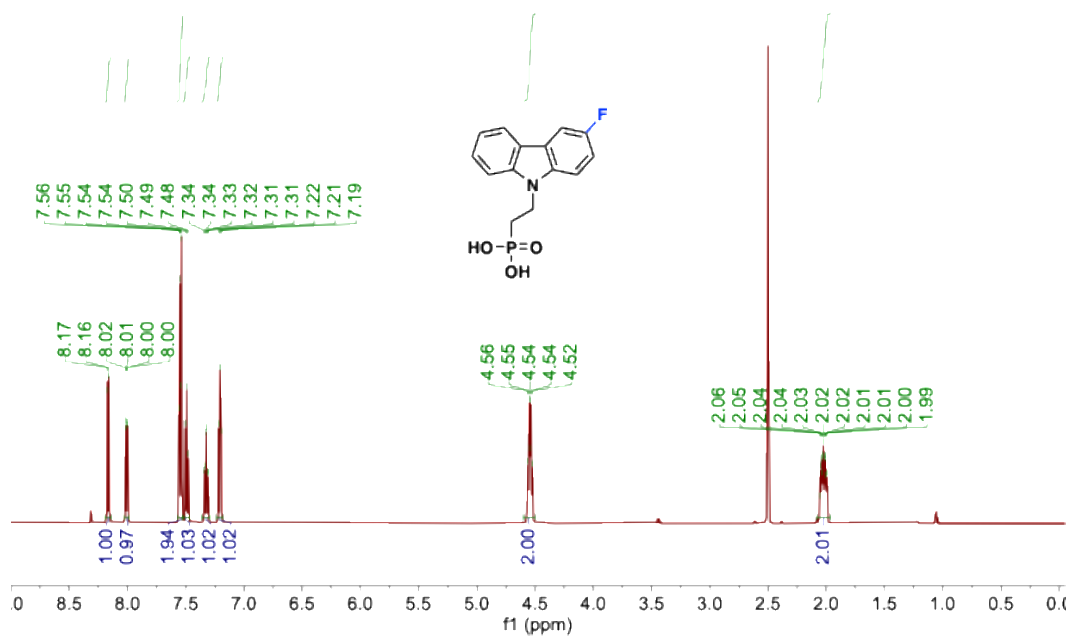


Figure S40. ^1H NMR spectrum (600 MHz) for **1F-2PACz** taken in $\text{DMSO-}d_6$ at 25 °C.

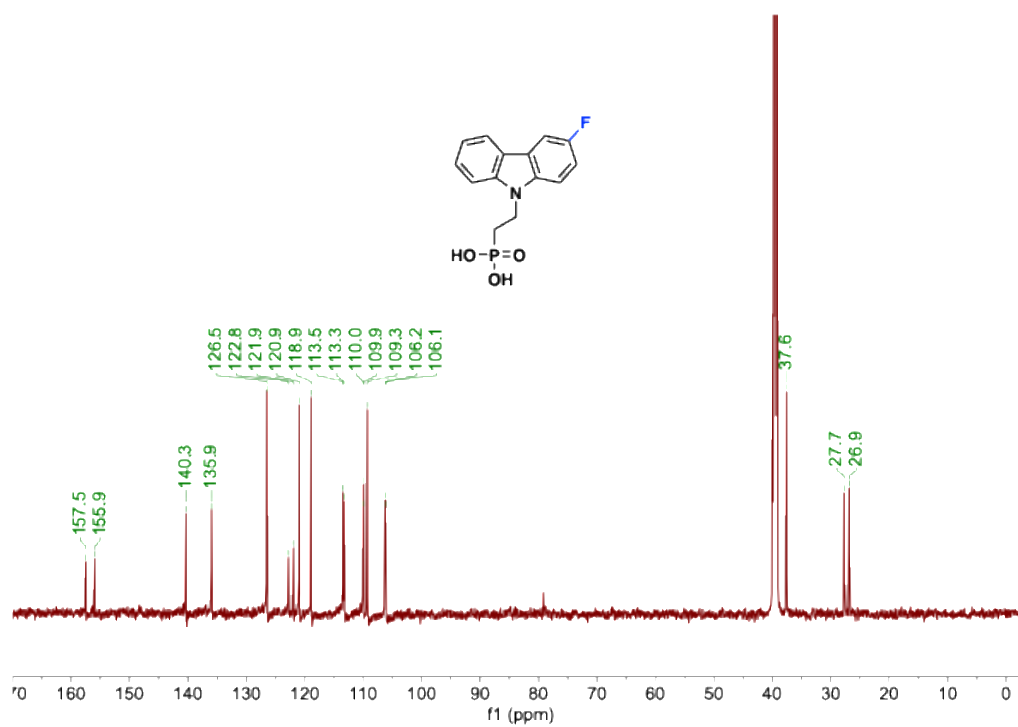


Figure S41. ^{13}C NMR spectrum (150 MHz) for **1F-2PACz** taken in $\text{DMSO-}d_6$ at 25 °C.

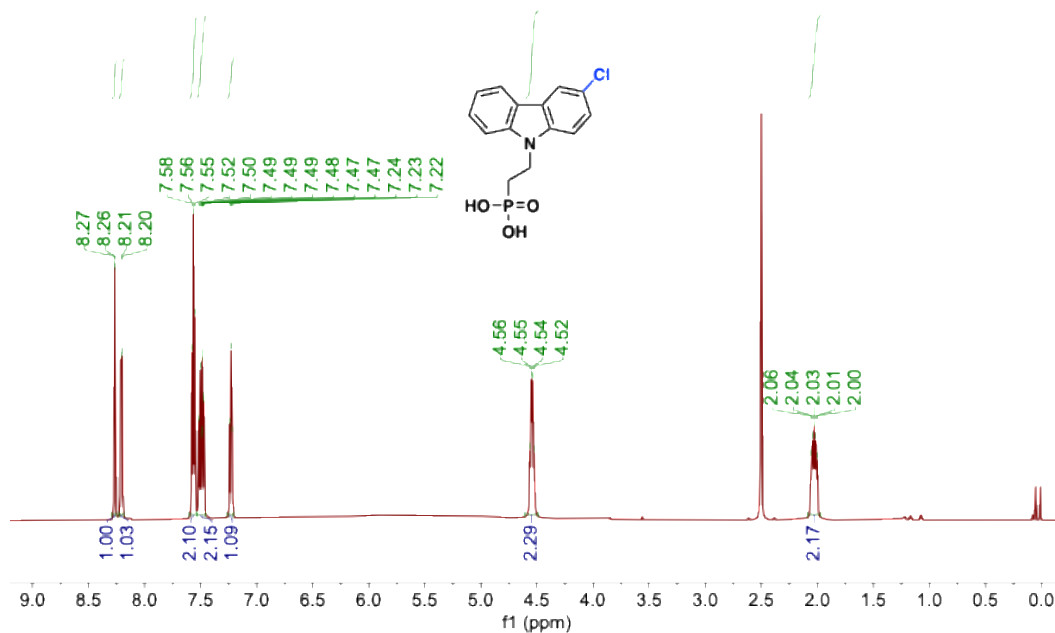


Figure S42. ^1H NMR spectrum (600 MHz) for **1Cl-2PACz** taken in $\text{DMSO-}d_6$ at 25 °C.

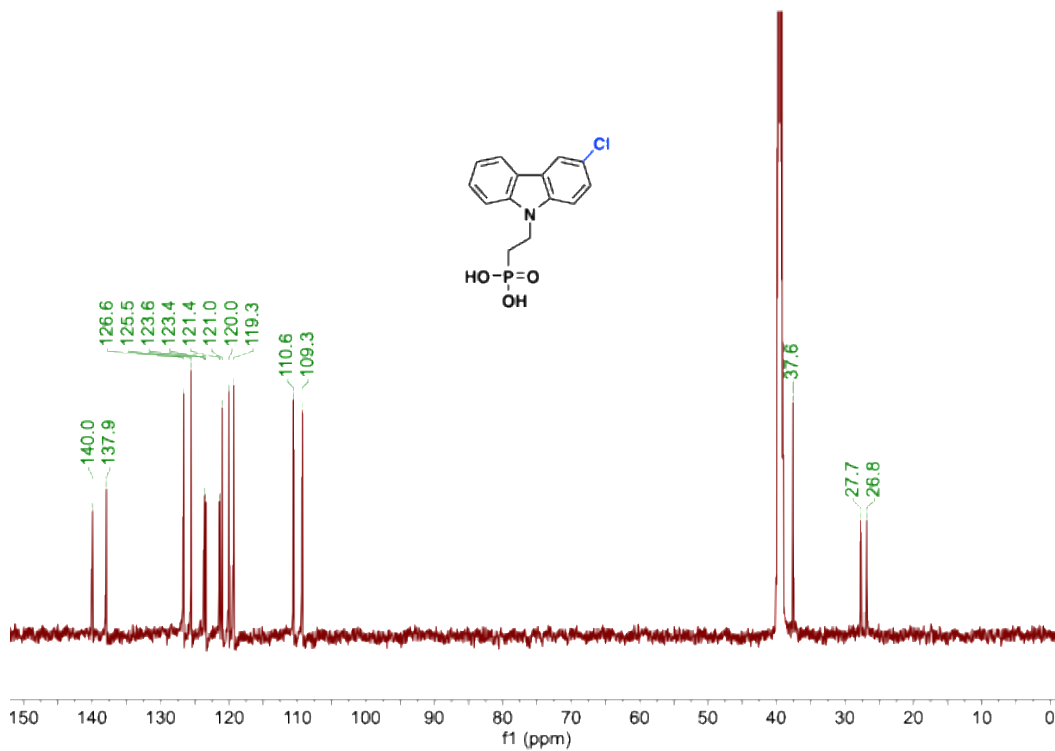


Figure S43. ^{13}C NMR spectrum (150 MHz) for **1Cl-2PACz** taken in $\text{DMSO-}d_6$ at 25 °C.

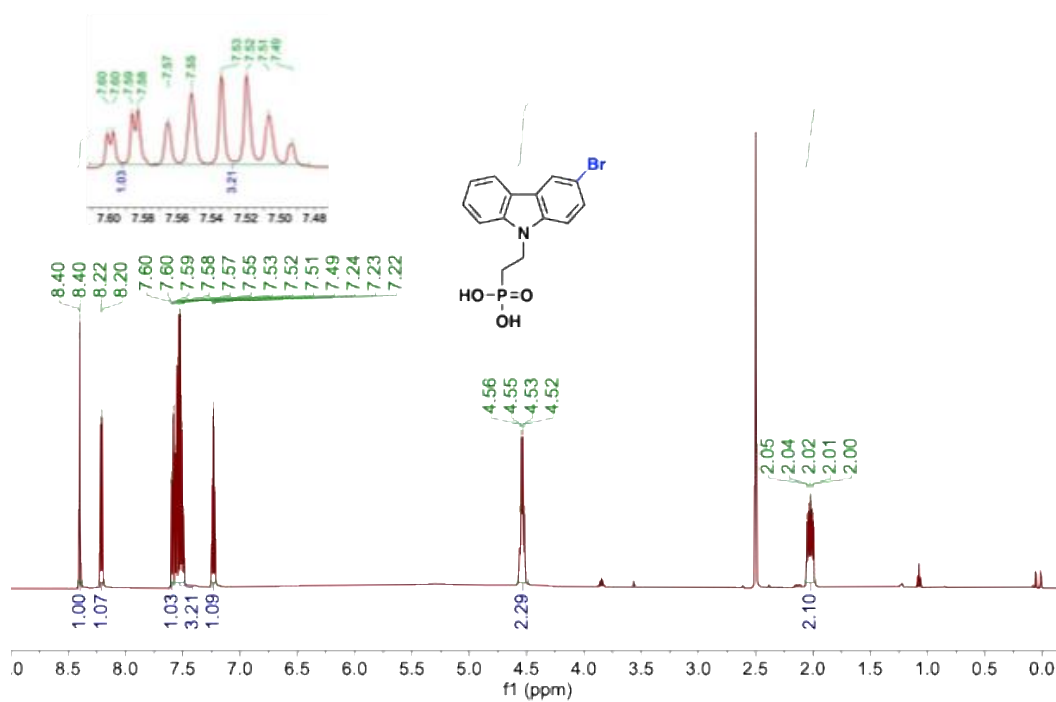


Figure S44. ^1H NMR spectrum (600 MHz) for **1Br-2PACz** taken in $\text{DMSO-}d_6$ at $25\text{ }^\circ\text{C}$.

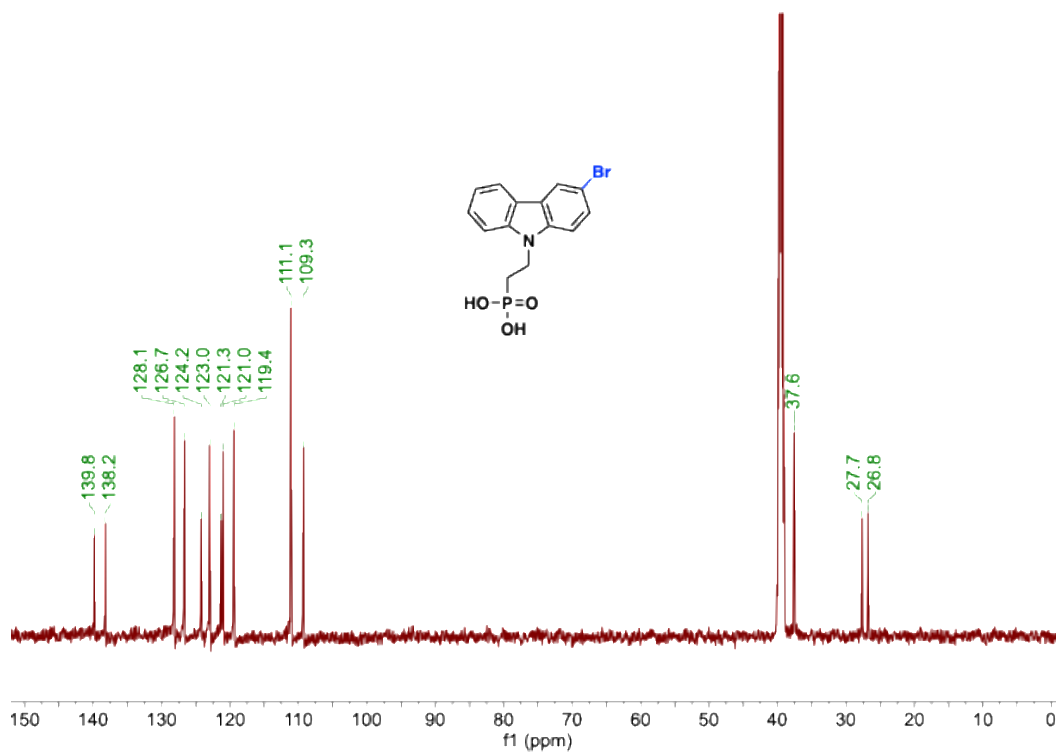


Figure S45. ^{13}C NMR spectrum (150 MHz) for **1Br-2PACz** taken in $\text{DMSO-}d_6$ at $25\text{ }^\circ\text{C}$.

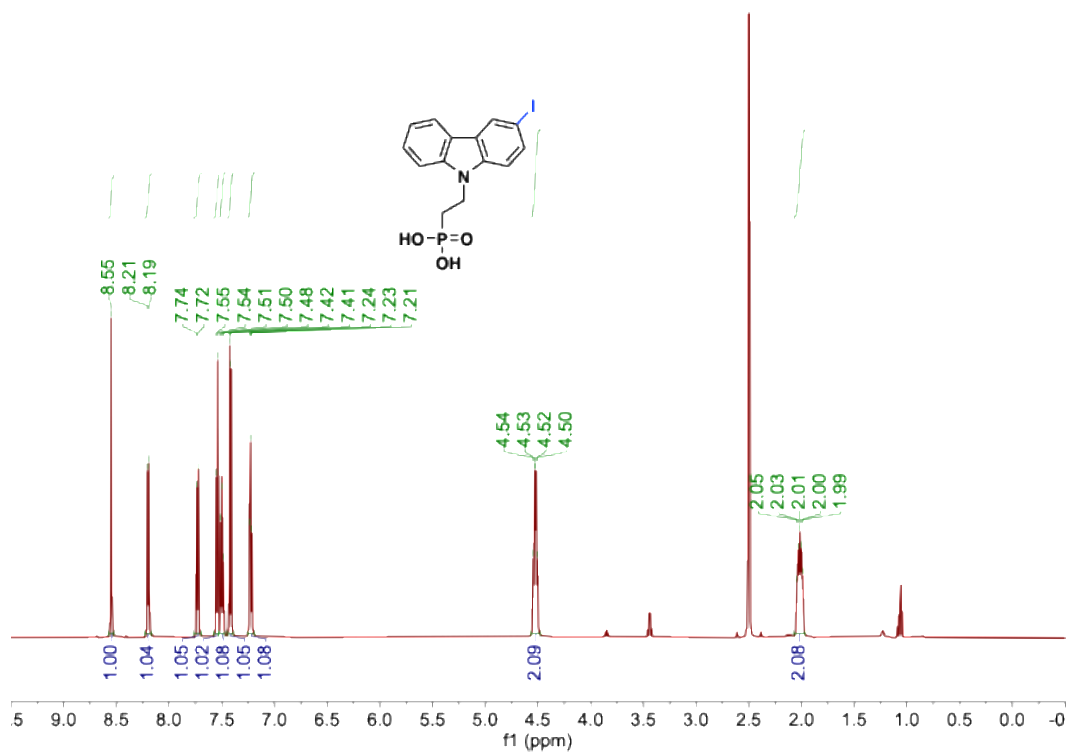


Figure S46. ^1H NMR spectrum (600 MHz) for **1I-2PACz** taken in $\text{DMSO-}d_6$ at 25 °C.

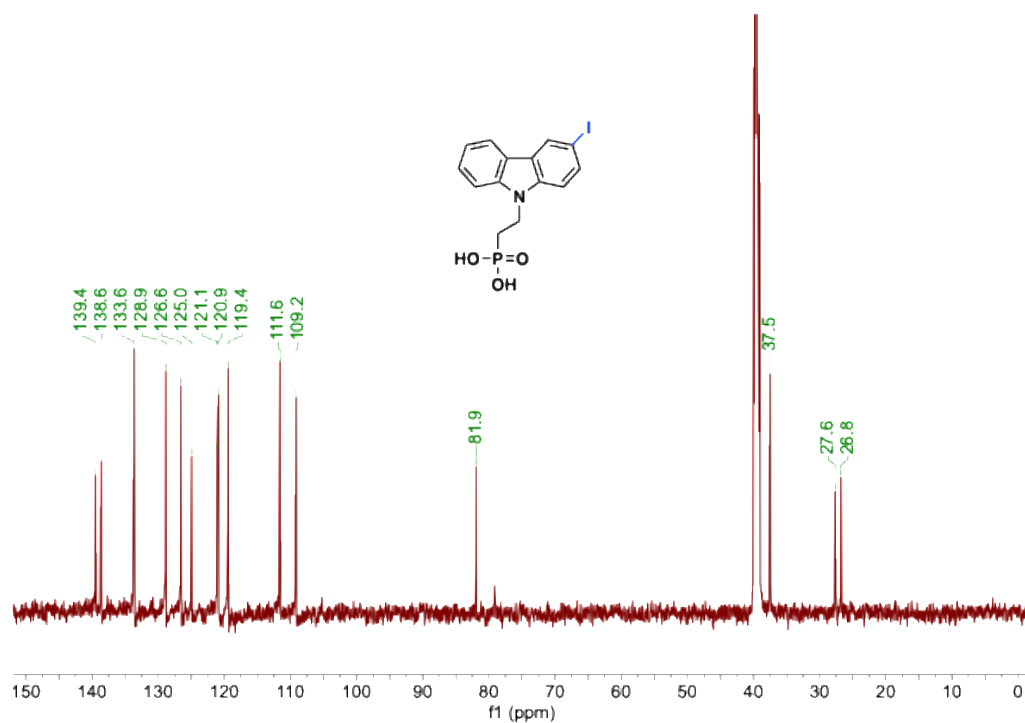


Figure S47. ^{13}C NMR spectrum (150 MHz) for **1I-2PACz** taken in $\text{DMSO-}d_6$ at 25 °C.

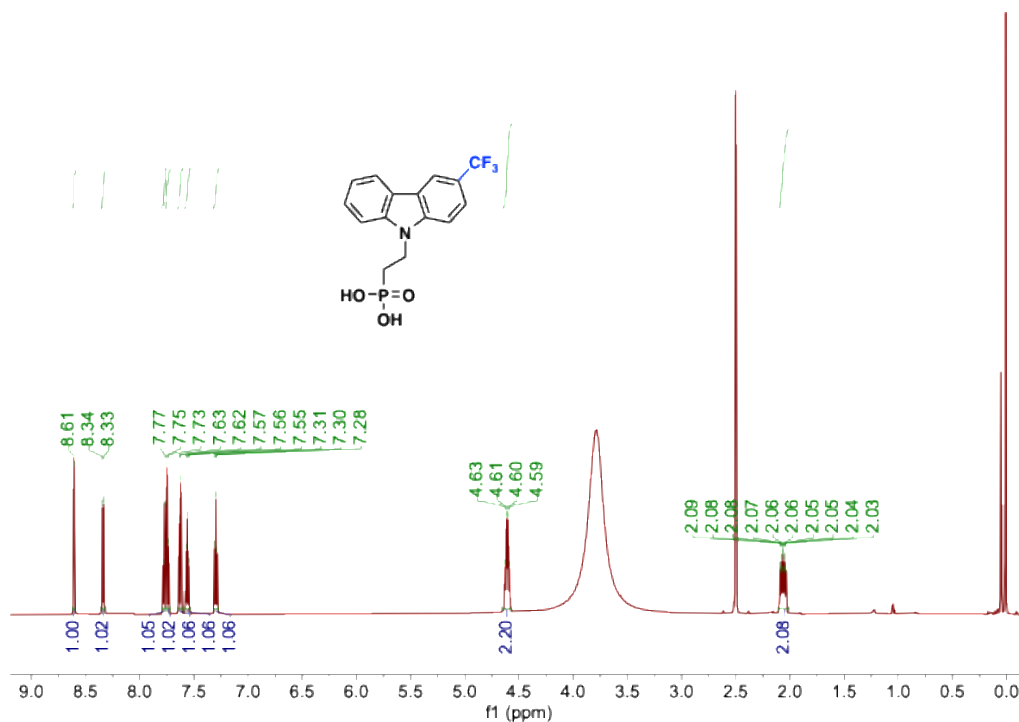


Figure S48. ¹H NMR spectrum (600 MHz) for 1CF₃-2PACz taken in DMSO-*d*₆ at 25 °C.

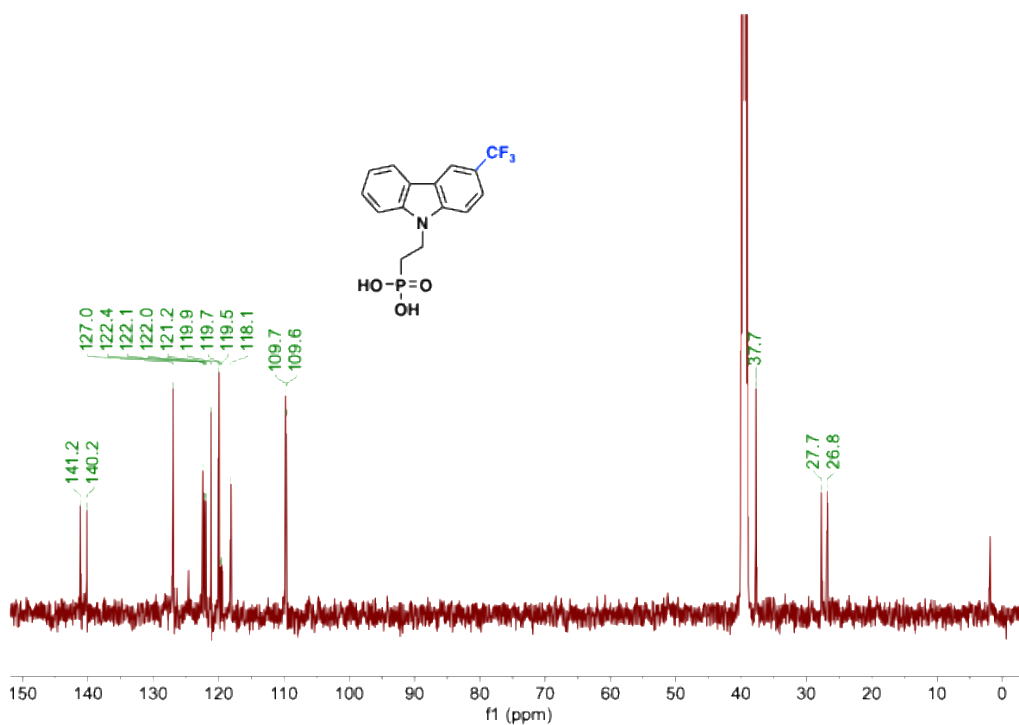


Figure S49. ¹³C NMR spectrum (150 MHz) for 1CF₃-2PACz taken in DMSO-*d*₆ at 25 °C.

5. Supplemental References

- (1) Dolomanov, O. V.; Bourhis, L. J.; Gildea, R. J.; Howard, J. A.; Puschmann, H. OLEX2: a complete structure solution, refinement and analysis program. *Applied Crystallography* **2009**, *42*, 339-341.
- (2) Becke, A. D. Density - functional thermochemistry. III. The role of exact exchange. *J. Chem. Phys.* **1993**, *98*, 5648-5652.
- (3) Weigend, F.; Ahlrichs, R. Balanced basis sets of split valence, triple zeta valence and quadruple zeta valence quality for H to Rn: Design and assessment of accuracy. *Phys. Chem. Chem. Phys.* **2005**, *7*, 3297-3305.
- (4) Frisch, M.; Trucks, G.; Schlegel, H.; Scuseria, G.; Robb, M.; Cheeseman, J.; Scalmani, G.; Barone, V.; Petersson, G.; Nakatsuji, H. Gaussian 16 Revision C. 01, 2016. *Gaussian Inc. Wallingford CT* **2016**, *1*, 572.
- (5) Perdew, J. P.; Burke, K.; Ernzerhof, M. Generalized gradient approximation made simple. *Phys. Rev. Lett.* **1996**, *77*, 3865.
- (6) Blöchl, P. E. Projector augmented-wave method. *Phys. Rev. B* **1994**, *50*, 17953.
- (7) Kresse, G.; Joubert, D. From ultrasoft pseudopotentials to the projector augmented-wave method. *Phys. Rev. B* **1999**, *59*, 1758.
- (8) Grimme, S.; Antony, J.; Ehrlich, S.; Krieg, H. A consistent and accurate ab initio parametrization of density functional dispersion correction (DFT-D) for the 94 elements H-Pu. *J. Chem. Phys.* **2010**, *132*, 154104.
- (9) Kresse, G.; Hafner, J. Ab initio molecular dynamics for open-shell transition metals. *Phys. Rev. B* **1993**, *48*, 13115.
- (10) Lin, Y.; Magomedov, A.; Firdaus, Y.; Kaltsas, D.; El - Labban, A.; Faber, H.; Naphade, D. R.; Yengel, E.; Zheng, X.; Yarali, E. 18.4% organic solar cells using a high ionization energy self - assembled monolayer as hole - extraction interlayer. *ChemSusChem* **2021**, *14*, 3569-3578.
- (11) Chen, Q.; Sun, K.; Franco, L. R.; Wu, J.; Ohrstrom, L.; Liu, X.; Gumbo, M.; Ozorio, M. S.; Araujo, C. M.; Zhang, G.; Johansson, A.; Moons, E.; Fahlman, M.; Yu, D.; Wang, Y.; Wang, E. Effects of Alkyl Spacer Length in Carbazole-Based Self-Assembled Monolayer Materials on Molecular Conformation and Organic Solar Cell Performance. *Adv. Sci.* **2025**, *12*, 2410277.
- (12) Wen, L.; Tang, L.; Yang, Y.; Zha, Z.; Wang, Z. Ligand-Free Pd-Catalyzed Domino Synthesis of Carbazoles via Dehydrogenative Aromatization/C (sp²)-C (sp²) Coupling Sequence. *Org. Lett.* **2016**, *18*, 1278-1281.